Urban Climate 56 (2024) 102061

Contents lists available at ScienceDirect

Urban Climate

journal homepage: www.elsevier.com/locate/uclim

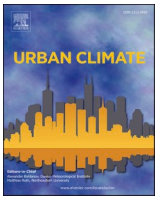

# Predicting urban Heat Island in European cities: A comparative study of GRU, DNN, and ANN models using urban morphological variables

Alireza Attarhay Tehrani [a], Omid Veisi [b,*], Kambiz kia [c], Yasin Delavar [d], Sasan Bahrami [e], Saeideh Sobhaninia [f], Asma Mehan [g]

[a] Department of Architecture, Faculty of Art and Architecture, South Tehran Branch, Islamic Azad University, Tehran, Iran
[b] Department of Information Systems and New Media, University of Siegen, Siegen, Germany
[c] The College of Architecture, Arts, and Design at Virginia Tech, Blacksburg, VA, USA
[d] University of Florida, College of Design, Construction and Planning, School of Architecture, Gainesville, USA
[e] Digital Media, Westphal College of Media Arts and Design, Drexel University, PA, USA
[f] School of Geographical Sciences and Urban Planning, Arizona State University, AZ, USA
[g] Huckabee College of Architecture, Texas Tech University, Lubbock, TX, USA

ARTICLE INFO

*Keywords:*
Urban heat island
Climate change
Deep learning
Sustainable development
Built environment

ABSTRACT

Continued urbanization, along with anthropogenic global warming, has and will increase land surface temperature and air temperature anomalies in urban areas when compared to their rural surroundings, leading to Urban Heat Islands (UHI). UHI poses environmental and health risks, affecting both psychological and physiological aspects of human health. Thus, using a deep learning approach that considers morphological variables, this study predicts UHI intensity in 69 European cities from 2007 to 2021 and projects UHI impacts for 2050 and 2080. The research employs Artificial Neural Networks, Deep Neural Networks, and Gated Recurrent Units, combining high-resolution 3D urban models with environmental data to analyze UHI trends. The results indicate strong associations between urban form, weather patterns, and UHI intensity, highlighting the need for customized urban planning and policy measures to reduce UHI impacts and foster sustainable urban settings. This research enhances understanding of UHI dynamics and serves as a valuable tool for urban planners and policymakers to address the challenges of climate change, urbanization, and air pollution, ultimately aiding in the improvement of health outcomes and building energy consumption. Moreover, the methodology effectively demonstrates the ability of the GRU to link its scores with UHI projections, offering crucial insights into potential health impacts.

## 1. Introduction

By 2050, a significant majority of the world's population will live in urban environments, a significant increase from the current 54%. In Europe, which is known as one of the most urban areas in the world, it has a staggering 73% urban population. This emphasizes the importance of urban development and climate adaptation strategies in Europe. In this way, it is very important to give priority to

* Corresponding author.
*E-mail addresses:* omid.veisi@student.uni-siegen.de, omid.veisi@mail.utoronto.ca (O. Veisi).

https://doi.org/10.1016/j.uclim.2024.102061
Received 12 February 2024; Received in revised form 1 May 2024; Accepted 6 July 2024
Available online 24 July 2024

**Nomenclature**

| Abbreviation | Description |
|---|---|
| *UHI* | *Urban Heat Island* |
| *UHIs* | *Urban Heat Island Intensity* |
| *HDD* | *Heating Degree Days* |
| *CDD* | *Cooling Degree Days* |
| *IQRs* | *Interquartile Ranges* |
| *AI* | *Artificial Intelligence* |
| *ML* | *Machine Learning* |
| *DL* | *Deep Learning* |
| *UWG* | *Urban Weather Generator* |
| *ANN* | *Artificial Neural Network* |
| *DNN* | *Deep Neural Network* |
| *GRU* | *Gated Recurrent Unit* |
| *SHAP* | *SHapley Additive exPlanations* |
| *LST* | *Land Surface Temperature* |
| *NDBI* | *Normalized Difference Built-up Index* |
| *NDVI* | *Normalized Difference Vegetation Inde* |
| *R2* | *R-Squared* |
| *MAE* | *Mean Absolute Error* |
| *MSE* | *Mean Squared Error* |
| *RMSE* | *Root Mean Square Error* |
| *PRelu* | *Parametric Rectified Linear Unit* |
| *tanh* | *hyperbolic tangent* |
| $\sigma$ | *sigmoid function* |
| $\phi$ | *hyperbolic tangent function* |
| $r_t$ | *reset gat* |
| $z_t$ | *update gate* |
| $h_t$ | *output* |
| $x_t$ | *input* |
| $\widehat{h}_t$ | *hidden state* |
| $h_{t-1}$ | *previous hidden state* |

favorable living conditions, including the adaptation of cities to climate changes, especially in the European continent, considering the high concentration of cities and its impact on global trends (Nastran et al., 2019; U. Nations, 2014; Mehan and Tafrata, 2023; Mehan, 2023; Varış Husar et al., 2023). In urban areas, heat stress is a growing concern (Lafortezza et al., 2009). The elevated surface and air temperatures in cities result from various factors such as land use, construction materials and urban morphology that is one of the most important key factors. Additionally, human activities that add heat (anthropogenic heat), and meteorological conditions like wind, humidity, sky view factor, radiation, and precipitation (Rizwan et al., 2008; Kleerekoper et al., 2012; Martin et al., 2015).

This increase in temperature in cities compared to rural environments, which occurs due to human climate changes, is called the Urban Heat Island (UHI) phenomenon, which is typical for dense urban areas (Schwarz et al., 2011; Schwarz et al., 2012). The challenges posed by UHI extend across different domains. Increasing demand for cooling systems increases energy consumption, which leads to increased costs and environmental impacts. In addition, UHI contributes to health issues with the potential for heat-related illnesses and disrupts ecosystems and adversely affects biodiversity (Arnfield, 2003). In Europe, many cities such as London, Paris, Madrid, Milan, etc. are struggling with distinct UHI challenges that are shaped by historical urban planning and climatic conditions (Guerreiro et al., 2018). With the intensification of urbanization, limited green space and sensitivity to heat waves complicates the reduction of UHI effects (Ahmed et al., 2020). The cooling impact of urban green spaces can extend from 200 to 400 m, varying based on their type and layout (Tyrväinen et al., 2005; Hamada and Ohta, 2010; Dugord et al., 2014; Monteiro et al., 2016). The presence and arrangement of green areas significantly influence the intensity of the UHI effect. However, it is important to consider not just their presence but also their distribution across the urban landscape (Maimaitiyiming et al., 2014). Studies indicate that a contiguous and densely vegetated green area plays a pivotal role in mitigating the UHI effect, offering more substantial cooling benefits compared to scattered smaller patches of greenery (Dugord et al., 2014; Chang et al., 2007; Cao et al., 2010).

The effects of the physical environment influence urban planning strategies and necessitate air quality management measures (Haas and Olsson, 2014). The challenges related to UHI in Europe require a different approach. As climate change accelerates, adaptation becomes essential for European cities. Integrating green spaces into urban planning seems to be a vital strategy to reduce the effects of UHI, provide areas for natural cooling and promote biodiversity. Addressing air quality concerns is critical, as UHI exacerbates pollution issues and affects respiratory health and overall urban well-being (Li et al., 2019; Ma et al., 2019; Heaviside et al., 2017).

Recent strides in artificial intelligence (AI), machine learning (ML), and deep learning (DL) technologies have revolutionized UHI forecasting (Fallah Madvari, 2022). These approaches harness data from diverse sources, including satellite imagery, weather stations, and urban sensors (Grêt-Regamey et al., 2021). By employing predictive modeling, these technologies analyze historical and real-time data to offer valuable insights into UHI patterns (Shi et al., 2021). The integration of AI/ML/DL in UHI forecasting aligns with the broader trend of leveraging technology to address intricate environmental challenges (Allam and Dhunny, 2019). This convergence empowers urban planners with the tools to make informed decisions, fostering sustainable urban development and resilience against the impacts of UHI (Mortaheb and Jankowski, 2023). Hence, harnessing AI solutions to analyze UHIs becomes invaluable for societal progress (Yang et al., 2020). Numerous studies have been undertaken to forecast UHIs (Lyu et al., 2022; Yao et al., 2020; Wang et al., 2024; Suthar et al., 2024). This study aims to enhance understanding of how different urban forms and structures contribute to UHI effects and to provide urban planners and policymakers with robust tools for predicting and mitigating these effects in the face of ongoing urbanization and climate change.

## 2. Literature review

### 2.1. Artificial intelligence and urban heat island

Studies focused on analyzing UHI phenomena involve a variety of data types due to the intricate and heterogeneous nature of urban environments. Conversely, ML and DL algorithms, such as random forests (Yao et al., 2020),support vector machines (Varentsov et al., 2023),Gradient Boosted models (McCarty et al., 2021),and Artificial Neural Networks (Liu et al., 2021),thrive on diverse datasets. The incorporation of various data types optimizes model performance (Qezelbash-Chamak et al., 2022), ensuring their effectiveness in capturing the complex patterns inherent in UHI phenomena. Researchers typically utilize a combination of satellite imagery, such as LandSATs (Liu et al., 2021; Rao et al., 2023; Vergara et al., 2023), land use/land cover (LULC) data (McCarty et al., 2021), meteorological data like air temperature, remote sensing data like LiDAR (Alonso and Renard, 2020), and urban morphological features to capture the inherent spatial and temporal variability of UHI effects. This multidimensional dataset is further enriched through multisensor data fusion techniques, as exemplified in the study by (Yao et al., 2020).In their investigation focused on Chengdu city in China, they advanced Land Surface Temperature (LST) estimation by integrating an ML algorithm and a spatiotemporal fusion model, achieving high spatial and temporal resolution. Integrating diverse data types and ML algorithms reveals previously unexplored dimensions of the UHI phenomenon, deepening our understanding of the built environment and its impact on local temperature variations.[41]emphasize the need to investigate spatiotemporal variations in LST and UHI indices. Their analysis of Baguio City exposes a worsening surface UHI associated with increased built-up areas. While LST layers alone prove unreliable as a UHI indicator due to weather conditions, the introduction of Random Forest regression, focusing on UHI indices such as the Normalized Difference Built-up Index (NDBI) and Normalized Difference Vegetation Index (NDVI), substantiates their claims. The role of ML algorithms in analyzing morphology has significantly advanced our comprehension of building structure, urban morphology, and land use dynamics (Zargar and Brown, 2020; Saldana Ochoa et al., 2021; Ochoa and Comes, 2021).In their study on extreme UHIs in factory areas, (Liu et al., 2021) utilized an Artificial Neural Network to assess factories' scale, shape, type, stage, and internal structure, correlating them with Land Surface Temperature (LST). The findings reveal that the scale and shape of factories directly impact LST, identifying optimal ranges for various land use categories and offering effective strategies to alleviate extreme UHIs. These results provide crucial theoretical guidance for resource-based cities addressing extreme heat.

The application of ML algorithms further enhances our understanding of the strong correlation between urbanization and land use land cover dynamics, influencing changes in LST, Park's Cooling Intensity (PCI), and UHIs (McCarty et al., 2021). Illustrated by the model of (Rao et al., 2023) for Imola City (1991–2021), changes in land use, such as converting green areas into agricultural land and constructing more buildings, significantly affect land temperature. This study contributes to our comprehension of how diverse land uses influence temperature variations in small cities, creating a more comprehensive understanding of the interconnected factors contributing to UHI.

### 2.2. Urban heat island and urban morphology

The investigation into UHIs encompasses a comprehensive exploration across various dimensions, necessitating an interdisciplinary approach. (Rizwan et al., 2008) serves as a pivotal foundation, emphasizing the indispensable nature of understanding urban morphology, land cover alterations, and anthropogenic heat sources in shaping UHI dynamics. (Mirzaei, 2015) sheds light on the intricate complexities encountered in accurately simulating UHIs, underscoring challenges arising from data requirements and the detailed nature of urban landscapes. Complementing this, (Stewart, 2011) highlights the need for standard methods to compare studies easily, addressing crucial gaps in methodologies employed within UHI research. Local contexts significantly influence UHI variations, evident in studies such as (Montávez et al., 2000; Touchaei and Wang, 2015) which show the strong effects of certain city environments on urban heat variations. In the realm of quantitative analysis of urban morphology, [50]is an important achievement, providing a strong method for studying urban form. Moreover, (Yuan et al., 2020) accentuates the importance of integrating urban morphology with heat management for developing effective mitigation strategies tailored to diverse urban settings. Studying UHI requires looking at them from many different fields and using various methods (Rizwan et al., 2008). The synthesis of findings from (Heaviside et al., 2017; Tan et al., 2010; Shahmohamadi et al., 2011; Piracha and Chaudhary, 2022) highlights the need to quickly reduce the impact of UHI on health with specific actions. These studies collectively underscore the heightened health risks posed by UHIs, ranging from heat-related illnesses to exacerbation of pre-existing conditions, especially in vulnerable populations residing in urban areas. Strategies

integrating urban planning, green infrastructure implementation, and heat mitigation measures highlighted in these works represent crucial pathways towards reducing the adverse health impacts of UHIs. Establishing resilient and health-conscious urban landscapes becomes imperative to shield communities from escalating health risks exacerbated by the UHI effect, thereby promoting well-being and fostering sustainable urban development.

The consequences of the UHI effect spread profoundly into public health, with a myriad of studies shedding light on its multifaceted impacts. Examining the connection between UHIs and health outcomes, (Wong et al., 2017) conducted a survey in Kuala Lumpur, highlighting the health implications faced by the working community due to heightened temperatures. Additionally, studies like (Klemm et al., 2015) underscore the significance of urban green spaces in mitigating the physical and psychological impacts of extreme heat during summertime. Understanding the spatial evolution of these effects, (Huang et al., 2020) emphasizes the dynamic relationship between UHIs and residents' health, defining how these spatial variations impact community well-being. Furthermore, the comprehensive review by (Singh et al., 2020) clarifies the intricate interplay between UHIs, air pollution, and climate change, collectively influencing human health in urban settings. Highlighting the tangible consequences, (Boned Fustel et al., 2021) analyzed the mortality rates in Valencia, Spain, revealing a stark correlation between the UHI effect and increased mortality rates. These studies collectively underscore the urgency of addressing UHI effects on human health, pushing for early actions to protect public health as city temperatures rise. Zooming into specific city dynamics, studies such as (Touchaei and Wang, 2015; Boukhabla et al., 2013) elucidate the intricate relationships between local morphology and UHI, demonstrating the critical influence of city-specific urban forms on heat island dynamics. Expanding these analyses to consider spatial heterogeneity (Liao et al., 2021; Huang and Wang, 2019) and broader

**Table 1**
Overview of Previous Studies on Machine Learning Methods for Urban Heat Islands.

| Authors | ML Method | Location | Metric | Findings |
|---|---|---|---|---|
| M. P. Taheri Otaghsara1 et al. (Taheri Otaghsara and Arefi, 2019) | PLS | Santa Rosa, California, USA | The R-square value of 0.81,The RMSE value of 1.02 | Land Surface Temperature is positively correlated with Index-based Built-up Index and Building Volume, but negatively correlated with Sky View Factor and Normalized Difference Vegetation Index. |
| Rao P. et al. (Rao et al., 2023) | N/S | Imola city, Italy | N/S | The study sheds light on the impact of varied land uses on temperature dynamics within small cities, noting transformations such as the conversion of green spaces to agricultural land and increased urbanization. Notably, the study's model underscores the influential role of land use types, particularly buildings and vegetation, in dictating land temperature variations. |
| Yan Liul et al. (Liu et al., 2020) | Numerical modeling | five cities(Not named) | N/S | Reducing building density has a more significant impact on mitigating the Urban Heat Island effect than reducing building height. |
| Neil Debbage, et al. ( Debbage and Shepherd, 2015) | Multivariate Regression Models | 50 most populous cities in the United States | N/S | The spatial contiguity of urban development, significantly influences the UHI effect and more discontiguous development pattern might help reduce UHI. |
| Ghiwa Assaf et al. (Assaf et al., 2023) | white-box Bayesian network model | New Jersey, USA | accuracy of 87.88% | The most accurate model, a tree-augmented Bayesian network, achieves an 87.88% accuracy in predicting UHI severity. |
| Vergara et al. (Vergara et al., 2023) | Random Forest regression | BAGUIO City, Philippines | R2 = 0.89, MSE = 0.006 | Based on the results of regression analysis using random forest, the NDBI-NDVI combined model proposed and used in this study can account for about 89% of UTFVI changes. |
| Geun Young Yun et al. ( Yun et al., 2020) | LSTM | Sydney, Australia | "R2 (training) = between 0.770 and 0.932,R2 (test) = between 0.841 and 0.924 | Using long-term air temperature records alongside a suitable forecasting architecture can yield dependable forecasts of the UHI. |
| Fitsum Tariku et al. ( Tariku and Gharib Mombeni, 2023) | ANN | Vancouver, Canada | MAE = 1.1 to 4.39,RMSE = 1.31 to 5.18 | UHI effect raised cooling energy demand by 23% and reduced heating energy consumption by 29%. |
| Varentsov, M et al. ( Varentsov et al., 2023) | RR, RFR, GBR, CBR, SVR, and MLPR | Moscow, Russia | RMSE of 0.7 and R2 > 0.8 | ML models, fueled solely by reanalysis data, performed better. However, over a longer time frame (1977 to 2023), ML models cannot fully replicate the observed increase in temperature difference, suggesting that urban growth plays an important role in this process. |
| Marjan Faraji et al. ( Faraji et al., 2022) | 3D CNN-GRU deep learning method LSTM, GRU, ANN, SVR, and ARIMA | Tehran, Iran | R2 = 0.84 | To showcase the suitability of the proposed model in the urban context, the study concentrates on air pollution data. |
| Addas, A. et al. (Addas, 2023) | bagging and random subspace | Jeddah, Saudi Arabia | N/S | Correlation analysis indicates impervious surfaces amplify UHI, while vegetation and water cover mitigate it. |

factors (Zhou and Chen, 2018) becomes instrumental for a holistic understanding. Further insights into UHI evaluation and human comfort are provided in (Steeneveld et al., 2011) while modeling approaches in (Yin et al., 2018) contribute nuanced perspectives. Moreover, (Fitria et al., 2019) delves into the intricate relationships between biophysical mechanisms, climate variations, and urban morphology, offering significant insights for comprehensive UHI mitigation strategies.

Quantifying the impacts of UHIs on human comfort and health is a multifaceted endeavor, illustrated by studies such as Steeneveld et al.'s quantitative assessment (Steeneveld et al., 2011) and Liu et al.'s multi-indicator investigation (Liu et al., 2023). These works provide nuanced insights into the quantifiable links between urban morphology, the prevalence of UHI effects, and their profound implications for human well-being. Wong et al.'s survey in Kuala Lumpur (Wong et al., 2017) underscores the direct health impacts experienced by urban populations due to heightened temperatures, highlighting the urgent need to address UHI effects on human health. Concurrently, Klemm et al. (Klemm et al., 2015) emphasize the role of urban green spaces in alleviating the psychological and physical effects of extreme heat, showcasing the pivotal role of urban design in enhancing outdoor thermal comfort. Huang et al.'s spatial analysis (Huang et al., 2020) further delineates the complex relationship between UHIs and residents' health, elucidating how differing urban landscapes influence these effects. Comprehensively, Singh et al.'s study (Singh et al., 2020) delves into the intricate nexus between UHIs, air pollution, and climate change, amplifying the collective impact on human health within urban environments. Moreover, Boned et al.'s analysis (Boned Fustel et al., 2021) of the UHI effect on mortality rates in Valencia reaffirms the urgency of addressing these impacts. Together, these studies accentuate the imperative of holistic urban planning strategies that consider both urban morphology and UHI effects to mitigate adverse health outcomes associated with intensified urban heat islands.

Kleerekoper et al., serves as a foundational cornerstone, emphasizing the critical importance of understanding urban morphology, alterations in land cover, and anthropogenic heat sources in shaping UHI dynamics (Kleerekoper et al., 2012). Diving deeper into the challenges faced in modeling UHIs, (Mirzaei, 2015) elucidates the complexities associated with accurately simulating these effects, grappling with intricate data requirements and the dynamic interactions within urban landscapes. Complementing this, (Stewart, 2011) highlights the importance of using standard methods to make strong comparisons between different studies, addressing pivotal gaps in methodologies employed within UHI research. Understanding the interplay between UHIs, urban morphology, and their impact on human health enables the prediction and proactive planning of health-oriented cities. This predictive ability holds immense significance in steering urban design towards fostering healthier environments. Studies such as Montávez et al.'s investigation (Montávez et al., 2000) and Touchaei et al.'s work (Touchaei and Wang, 2015) highlight the contextual intricacies influencing UHI variations, demonstrating the profound impact of specific urban settings on the variability of heat islands. Within the domain of quantitative urban morphology analysis, Fleischmann et al.'s methodology (Fleischmann, 2019) stands as a breakthrough, offering a robust framework for evaluating urban form. Additionally, Yuan et al.'s research (Yuan et al., 2020) underscores the pivotal fusion of urban morphology and efficient heat management, crucial for devising tailored mitigation strategies that suit diverse urban settings. The ability to predict UHI dynamics and their relationship to urban morphology not only aids in city planning but also lays the foundation for crafting health-centric urban landscapes, aligning with the imperative of fostering well-being within urban communities. Table 1 provides a brief overview of previous studies regarding Machine Learning methods for addressing urban heat islands.

### *2.3. Research gaps*

Through a comprehensive review of the existing literature, this study identifies significant gaps in research on predicting UHIs. Despite the continuous development of new machine learning (ML) algorithms, the need to determine the most effective approach for predicting UHIs is very important. In addition, some advanced DL techniques, such as GRU, commonly used for time series modeling, and deep neural networks, have not yet been used to predict UHIs, which is a complex climate-anthropogenic issue.

To address these research gaps, our study focuses on predicting this phenomenon using four advanced DL techniques: ANN, DNN, and GRU, each representing a complex DL model. The first goal of this study is to compare the performance of DL models to accurately predict this phenomenon and to identify the best model for this purpose.

The second research gap identified in past studies is the effect of urban characteristics on performance and UHI. The characteristics of the urban area directly affect the control of radiation intensity and ambient temperature on the Earth's surface, but previous research ignored their importance by considering them as independent variables.

The third research gap identified in past studies is considering the prospect of increasing urban population in Europe in the coming years. It is important to simulate and investigate the intensity of the UHI for the years 2050 and 2080 according to the existing conditions of European cities, which previous studies have ignored.

To address this gap, our study examines how much the intensity of UHI increases in each European city in 2050 and 2080 and what is the effect on the increase and decrease of heating degree days and cooling degree days that have a direct effect on energy consumption in cities.

## 3. Research methodology

The proposed approach employs a parametric and architect-friendly process that uses open-access repositories such as the OpenStreetMap dataset, along with a Building Energy Model-Town Energy Balance tool known as UWG. Thus, a distinctive methodology was devised, employing the concept of parameter and indicator selection tailored to the size of the city. Parametric modeling and the analysis of UHIs were specifically designed for urban scale. In the initial stage of the research, the Elk plugin was utilized to simulate urban morphology, generating a comprehensive parametric model that incorporated factors such as building heights, volumes, green space, and x and y coordinate points. These parameters were extracted from an openly accessible repository like the


| Country : Austria | Country : Belgium | Country : Croatia | Country : Bulgaria |
|---|---|---|---|
| 1 City: Linz | 4 City: Brussels | 7 City: Rijeka | 10 City: Burgas |
| 2 City: Salzburg | 5 City: Ghent | 8 City: Varazdin | 11 City: Ruse |
| 3 City: Vienna | 6 City: Ostend | 9 City: Zagreb | 12 City: Sofia |
| **Country : Portugal** | **Country : Romania** | **Country : Spain** | **Country : Sweden** |
| 13 City: Faro | 16 City: Brasov | 19 City: Barcelona | 22 City: Goteborg |
| 14 City: Lisbon | 17 City: Bucharest | 20 City: Madrid | 23 City: Malmo |
| 15 City: Porto | 18 City: Cluj-Napoca | 21 City: Valencia | 24 City: Stockholm |
| **Country : Cyprus** | **Country : Czech** | **Country : Poland** | **Country : Netherlands** |
| 25 City: Grine | 28 City: Olomouc | 31 City: Lublin | 34 City: Amsterdam |
| 26 City: Guzelyurt | 29 City: Plzen | 32 City: Poznan | 35 City: Eelde |
| 27 City: Nicosia | 30 City: Prague | 33 City: Warsaw | 36 City: Rotterdam |
| **Country : Ireland** | **Country : Latvia** | **Country : Lithuania** | **Country : France** |
| 37 City: Birr | 40 City: Dobele | 43 City: Kaunas | 46 City: Marseille |
| 38 City: Cork | 41 City: Madona | 44 City: Palanga | 47 City: Paris |
| 39 City: Dublin | 42 City: Riga | 45 City: Vilnius | 48 City: Rennes |
| **Country : Hungary** | **Country : Greece** | **Country : Germany** | **Country : Denmark** |
| 49 City: Budapest | 52 City: Athens | 55 City: Frankfurt | 58 City: Aalborg |
| 50 City: Eger | 53 City: Chios | 56 City: Hamburg | 59 City: Copenhagen |
| 51 City: Sopron | 54 City: Patras | 57 City: Munich | 60 City: Roskilde |
| **Country : Estonia** | **Country : Finland** | **Country : Italy** | |
| 61 City: Parnu | 64 City: Tampere | 67 City: Bologna | |
| 62 City: Tallinn | 65 City: Oulu | 68 City: Milan | |
| 63 City: Tartu | 66 City: Helsinki | 69 City: Rome | |

*(caption on next page)*

**Fig. 1.** The location of cities.

OpenStreetMap dataset. The created parametric model became the basis for running energy simulations afterward.

In this study, 69 cities were examined in the European region shown Fig. 1. Later step involved estimating the UHIs by the UWG. This tool provides urban weather data in an epw format, suitable for use in energy simulation programs, featuring adjusted temperature and humidity influenced by the surrounding built environment. A large dataset was generated by integrating data from 69 cities in the European region. Each data source contained numerous independent variables and a dependent variable, including x and y coordinates, green space, azimuth angle, facade-to-site ratio, average height, building density, average volume, occupied area, unoccupied area, and the dependent variable was the mean UHI per year. In the next step, different cities were created to develop a huge dataset. We created an extensive dataset with 604,441 rows and 10 columns, facilitating the analysis of UHIs in the European region within urban environments.

The third phase corresponds to the pre-processing step of data for the AI models used in forecasting UHI. It involved three tasks, including removing outliers, normalizing data, and selecting features. These tasks aimed to enhance the quality and relevance of the data for the models. In the fourth step, as illustrated in the flowchart, our study involved a comparison of four distinct DL algorithms to determine the most effective model. Following the training, testing, and evaluation processes, it was identified that the GRU model emerged as the most proficient Fig. 2.

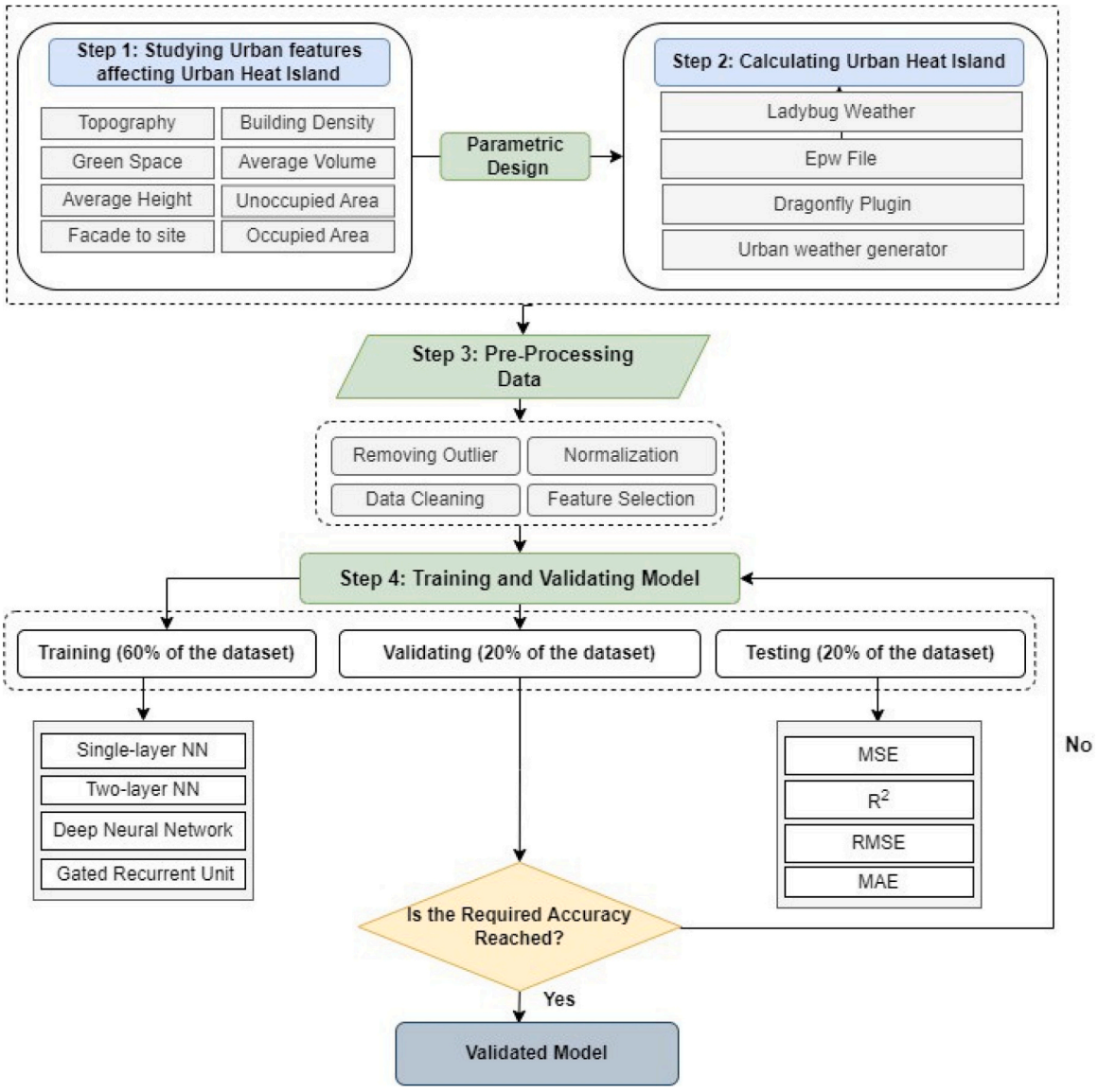


**Fig. 2.** The specifics of each stage and the practical tools associated with them are further explored in the subsequent sections.

### 3.1. Parametric modeling techniques

Parametric modeling is a design process that enables the alteration of a model's geometry by adjusting its dimension values. It facilitates the exploration of various design scenarios by integrating geometry variables and rules in an iterative design process. Integral to computational design, parametric models harness the power of AI and advanced mathematics to craft complex forms intricately. This approach involves the implementation of computer programming, such as scripting, to precisely define the dimensions and geometry of the model, showcasing the intersection of technology and design innovation (Burry and Kolarevic, 2003). Parametric design transforms the design process into a parametric model, capable of influencing the production of a design outcome by adjusting parameters. This innovative design approach enhances designers' adaptability to complex environments, fostering the creation of novel objects and introducing fresh perspectives to the design process. Emphasizing interdisciplinary collaboration, parametric design's internal complexity, diversity, and inclusiveness significantly impact traditional design methodologies, bringing about substantial shifts in people's perspectives (Han et al., 2023). The objective of this research is to create a data-driven parametric methodology for measuring UHI at the convergence of urban design and architectural intricacies.

In the initial phase, the integration of the 3D model into the UWG program involved a thorough assessment of the land uses in the area. Each building's function in the model, whether residential, commercial, industrial, civic, institutional, open space, unoccupied area, cemetery, or water, was individually assigned. It allows for the evaluation of anthropogenic heat emissions and internal heat accumulation within individual clusters of buildings, including residential, commercial, mixed-use, etc., independently for each specific region when implementing the UWG model. The accurate 3D modeling and integration into the UWG were achieved using a combination of Grasshopper 3D, the Elk plug-in, and an openly accessible repository like the OpenStreetMap dataset. Additionally, it facilitated the calculation of hourly values for urban air temperature and humidity through the UWG. The workflow outlined in this step is universally applicable to any location with available OpenStreetMap data. Building footprints, parcels, and green spaces used in modeling 69 cities were extracted from the OpenStreetMap dataset. The resulting 3D model is depicted in Fig. 3.

### 3.2. Urban Heat Island calculating

In this study, the calculation of UHIs was conducted utilizing the UWG. To determine UHIs, 3D models representing urban blocks, along with their essential features, were provided as inputs to the UWG for each specific region. The study employed Rhinoceros version 7.0 for this purpose. The UWG model utilizes weather data from an operational station situated outside the city to estimate air temperatures within urban canyons. Specifically, the Dragonfly version of the UWG plug-in for Rhinoceros was utilized in this research. The reference weather data spanned the Typical Meteorological Year 3 (TMY 3) from 2007 to 2021. The reference temperature was obtained from the hourly dry-bulb temperature within the epw file. UHIs calculations involved running the UWG model for each region to estimate the urban canopy temperature. Determining UHIs relied on the temperature difference between the simulated temperature for each region and the TMY data. The UWG model simulated UHIs for each region for a whole year, providing results in epw format as a Precise measure of UHIs (1).

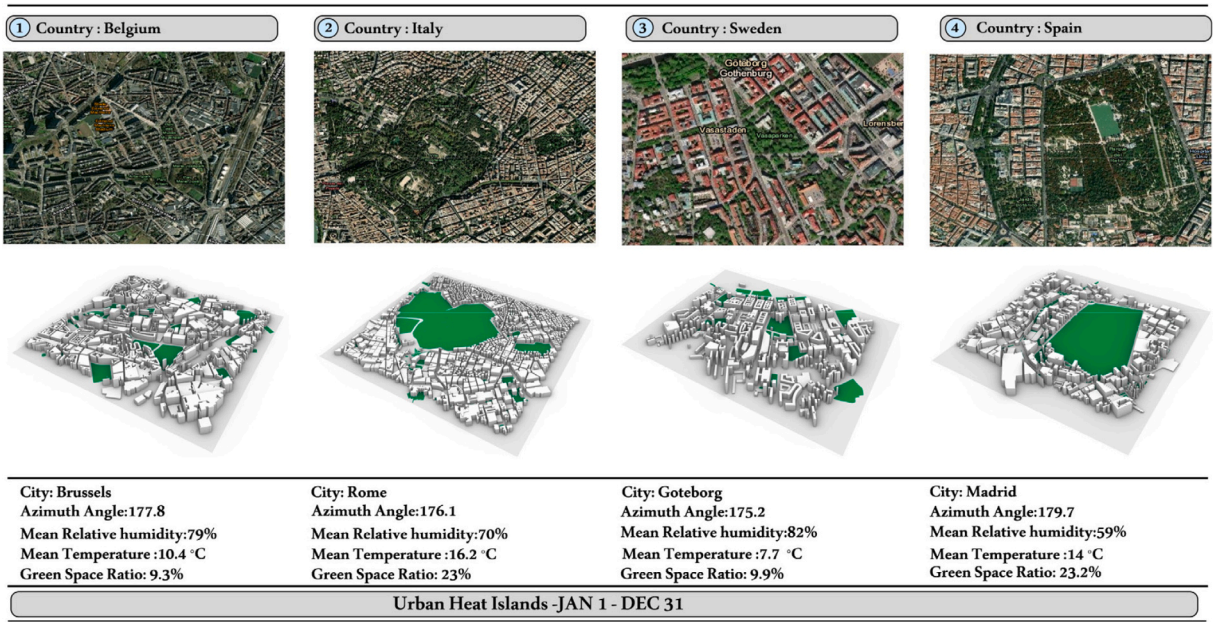


**Fig. 3.** 3D model of cities.

**Algorithm 1**. Simulation Workflow.
**procedure** NAME(Parametric design).

2: *X*←*define*(*open street map data*)
*X*←*define*(*design variables*).
4: *epw*←*read*(*EPW file*)
*Urbantexture*←*define*(*Dragonfly Plugin*).
6: *Transform masses to zones*
*Set the Unoccupied Area.*
8: *Set the occupied area*
*Set the building density.*
10: *Set average Hieght*
*Set Average volume.*
12: *Set green space*
*conditions*←*set*(*Urban Area boundary conditions).*
14: $UA_{\text{params}}$←*set*(*urban heat island parameters*)
*Set UA construction.*
16: Set City on topology
end procedure.
18: **procedure** NAME(*Compute objective functions*).
**function F** $_1$(*X*,*epw*,*conditions*,$UA_{\text{params}}$).
20: *Generate open street map on location*
*Create Polyline based on OSM Data.*
22: *profile results.*
*Return Building density.*
24: *Return unoccupied area*
*Return Occupied Area.*
26: **return Return Average Hieght.**
**end function.**
28: **function F**$_2$(*X*,*epw*,*conditions*,$UA_{\text{params}}$).
*Generate Urban Area.*
30: *Set EPW file*
*Run UWG for Analysising.*
32: *Read the required annual UHI simulation*
*Generate UHI intensity.*
34: *Generate CDD and HDD*
**(return) SR$_{\text{avg}}$**
36: **end function.**

### *3.3. Dataset and geographic scope*

Urban morphological factors were derived from the dataset as input data in this investigation, subsequent to the computation of UHIs, with UHIs functioning as the output data. Topographical characteristics (X and Y point coordinates), azimuth angle, facade-to-site ratio, unoccupied area, occupied area, average building heights, average building volumes, building density, and green space were all included in the dataset. The aforementioned were designated as independent input variables, whereas the sole output variable comprised UHIs data collected from 69 localities throughout the European continent. The cities were chosen with the intention of representing a broad spectrum of climates, as classified by the Koeppen climatic system. The dataset was systematically collected to guarantee that it encompassed a wide range of climatic zones, thereby enabling a thorough and comprehensive analysis.This study involves the benchmarking of climate classifications for various European cities based on the Köppen climate classification system. With the Koppen classification, a comprehensive summary of the climatic conditions in each city is available. Cfb (Warm summer continental or hemiboreal), Cfa (Humid subtropical), Csa (Mediterranean), Dfb (Warm summer continental or hemiboreal), BSh (Hot semi-arid), Csb (Warm summer Mediterranean climate), and Dfc (Subarctic) are the various climatic zones through which the cities are dispersed. Each of the communities in this assortment symbolizes a distinct climatic zone. This research utilized two independent variables as inputs for the dataset, which comprised topographic features denoted by X and Y coordinate points. The coordinates in question represent the precise whereabouts of a point on the ground. They are established upon a reference system that partitions the planet into a horizontal and vertical grid. Each city is designated by a unique set of coordinates, with each x and y coordinate serving as an indicator of its location.

Green space is the significant independent variable under investigation in this study. Additionally, green space is a crucial component of urban morphology. The distribution, location, size, and configuration of green space can have an effect on the UHI effect. Building density also influences the intensity of UHI by influencing the quantity of heat that urban structures absorb and retain. Because it diminishes ventilation and heat evaporation and increases the surface area exposed to solar radiation, a greater building

density may result in greater UHI effects (Giridharan et al., 2004). An additional pivotal independent variable being examined in this study is the mean height of structures. In order to guarantee a precise simulation of every city, the vertical extent of structures was simulated within the urban texture. Due to the fact that the building heights in each urban area were distinct and varied, the simulations became more complicated. Furthermore, the inclusion of building volume as a crucial element in the UHI estimation model that was constructed for this research serves to supplement the building height analysis. The volume of structures has a substantial impact on the manner in which solar radiation is absorbed and reflected by building surfaces; consequently, this contributes to the overall disparity in temperature between urban and rural regions (Veisi et al., 2022). In this research, the azimuth angle is of critical importance in the simulation model that has been developed to analyze the UHI phenomenon. It functions as a critical parameter, specifying the orientation of a particular location on the surface of the Earth in relation to the sun. The variation in this angle can be attributed to temporal and geographical factors that differ between regions. A meticulous determination of an exhaustive range of azimuth angles was conducted for all 69 cities spanning the European continent in the course of this study. We incorporated two additional variables, occupied and unoccupied areas, as inputs to our simulation model in our research. The term "occupied area" denotes the cumulative extent of buildings and structures that are present on an urban site, whereas "unoccupied area" comprises the residual vacant space. In the context of the UHI effect, unoccupied and occupied areas are significant because they influence the quantity of heat absorbed, reflected, and discharged by the urban surface.

### 3.4. Data preprocessing

In the dataset preprocessing phase, we employed the Min-max scaler technique as a normalization method to standardize variable values within the 0 to 1 range. This process entails subtracting the minimum value and dividing by the variable's range. Min-max scaler is especially advantageous for datasets with fixed ranges, such as percentages or ratings. Its application aims to improve the performance and accuracy of ML models by mitigating the impact of outliers or extreme values that could distort results. Moreover, Min-max scaler contributes to reducing computational costs and model complexity, simplifying and accelerating calculations.

During the dataset construction for UHI calculation using the UWG, two variables, namely Tree Coverage Ratio and Grass Coverage Ratio, initially played a pivotal role in assessing UHIs. However, in the dataset creation phase, given the nature of Urban Morphology data, we employed a strategic feature selection approach after data normalization. Notably, Feature selection involved excluding these two variables to streamline the dataset for the specific objectives of this study. This decision was made to prioritize and retain the most influential variables while minimizing redundancy and ensuring the dataset's relevance to the research goals. This meticulous feature selection process, contributes to optimizing the dataset, aligning it more closely with the targeted output of the investigation.

### 3.5. Deep learning algorithms

#### 3.5.1. Artificial neural network

In our research, four DL algorithms are used for protecting UHI based on urban morphology variables. First, two ANN models have been employed to address the research problem. ANN, a subset of AI, serve as powerful computational models inspired by the intricate architecture of biological neural networks (Sun et al., 2020). They function as robust research tools, proficient in tasks such as estimating nonlinear functions, categorizing data, recognizing patterns, optimizing processes, and forming clusters (Tehrani et al., 2024). The first model is a Single-layer ANN characterized by a simpler architecture with only one hidden layer, and it includes 50 neurons in this layer. On the other hand, the second model is a more complex Two-layer ANN with two hidden layers. The first hidden layer of this model encompasses 70 neurons, while the second hidden layer comprises 30 neurons. Both models share common training configurations, including a batch size of 128 and 50 epochs. The optimization process for both models is carried out using the Adam optimizer Table 2.

#### 3.5.2. Deep neural network

A DNN stands out as a sophisticated type of ANN, distinguished by its arrangement of neurons into multiple layers (Sun et al., 2020). In the context of a DNN, each neuron within a layer receives input from the neuron activations of the previous layer and executes a fundamental calculation (Tavares et al., 2022). The notable advantage of DNN over ANN lies in its ability to represent complex functions with fewer neurons, thereby reducing the risk of overfitting and enhancing generalization. Consequently, The DNN proves more powerful and efficient than ANN when it comes to addressing complex problems (Goodfellow et al., 2016). The DNN presented in this paper is structured with an input layer, five hidden layers, and an output layer Table 2. The hidden layers consist of

**Table 2**
Hyperparameter of the used models.

| Model | Gated Recurrent Unit | Deep Neural Network | Two-layer ANN | Single-layer ANN |
|---|---|---|---|---|
| Number of hidden layers | 8 | 5 | 2 | 1 |
| Number of neurons | (1024,512,256,128,64,32,32,16) | (200,80,80,80,80) | (70,30) | (50) |
| Number of batch size | 128 | 128 | 128 | 128 |
| Number of epoch | 50 | 50 | 50 | 50 |
| Optimizer | Adam | Adam | Adam | Adam |
| Activation function | tanh | PReLU | PReLU | PReLU |

200, 80, 80, 80, and 80 neurons, respectively. With a batch size of 128, it undergoes training over 50 epochs using the Adam optimizer. It is worth noting that the DNN, Single-layer, and Two-layer ANN all employ the Parametric Rectified Linear Unit (PReLU) as their activation function. In this study, the PReLU activation function was utilized for all three Neural Networks models.

### 3.5.3. Gated recurrent unit

Finally, The GRU, introduced by Cho et al. in 2014 (Cho et al., 2014), it is a specific kind of recurrent neural network (RNN). This model employs two essential gates, namely reset and update, to manage the information transfer from previous hidden states to the current one. Notably, GRU exhibits a streamlined and faster structure compared to the Long Short-Term Memory (LSTM) model, another variant of recurrent neural networks (Weiss et al., 2018; Faisal et al., 2022). The mathematical formulations that describe how the GRU works are shown in Eq. 1, Eq. 2, Eq. 3, and Eq. 4.

$$r_t = \sigma(w_r x_t + U_r h_{t-1} + b_r) \tag{1}$$

$$z_t = \sigma(w_z x_t + U_z x h_{t-1} + b_z) \tag{2}$$

$$\widetilde{h}_t = \phi\left(w^h x_t + U^h (r_t \odot h_{t-1}) + b^h\right) \tag{3}$$

$$h_t = (1 - z_t) \odot h_{t-1} + z_t \odot \widetilde{h}_t \tag{4}$$

Here, $r_t$ represents the reset gate, $z_t$ is the update gate, $h_t$ is the output, and $x_t$ represents the input. Additionally, $\widetilde{h}_t$ is the candidate hidden state. The weights for the update gate, reset gate, and candidate hidden state are denoted as $w_r$, $w_z$, and $w^h$ respectively. The previous hidden state is represented by $h_{t-1}$. The bias vectors for the update gate, reset gate, and candidate hidden state are $b_r$, $b_z$, and $b^h$ respectively. The sigmoid function ($\sigma$) is utilized to compress values between 0 and 1, while the hyperbolic tangent function ($\phi$) compresses values within the range of $-1$ to 1. Fig. 4 illustrates the architecture of a GRU. Our GRU-based network consists of eight layers, each with a different number of neurons, ranging from 1024 to 16 which has a total of 6,339,953 trainable parameters Table 3. A batch size of 128 is used and Adam is used as a gradient descent optimization algorithm, like the previous networks The activation

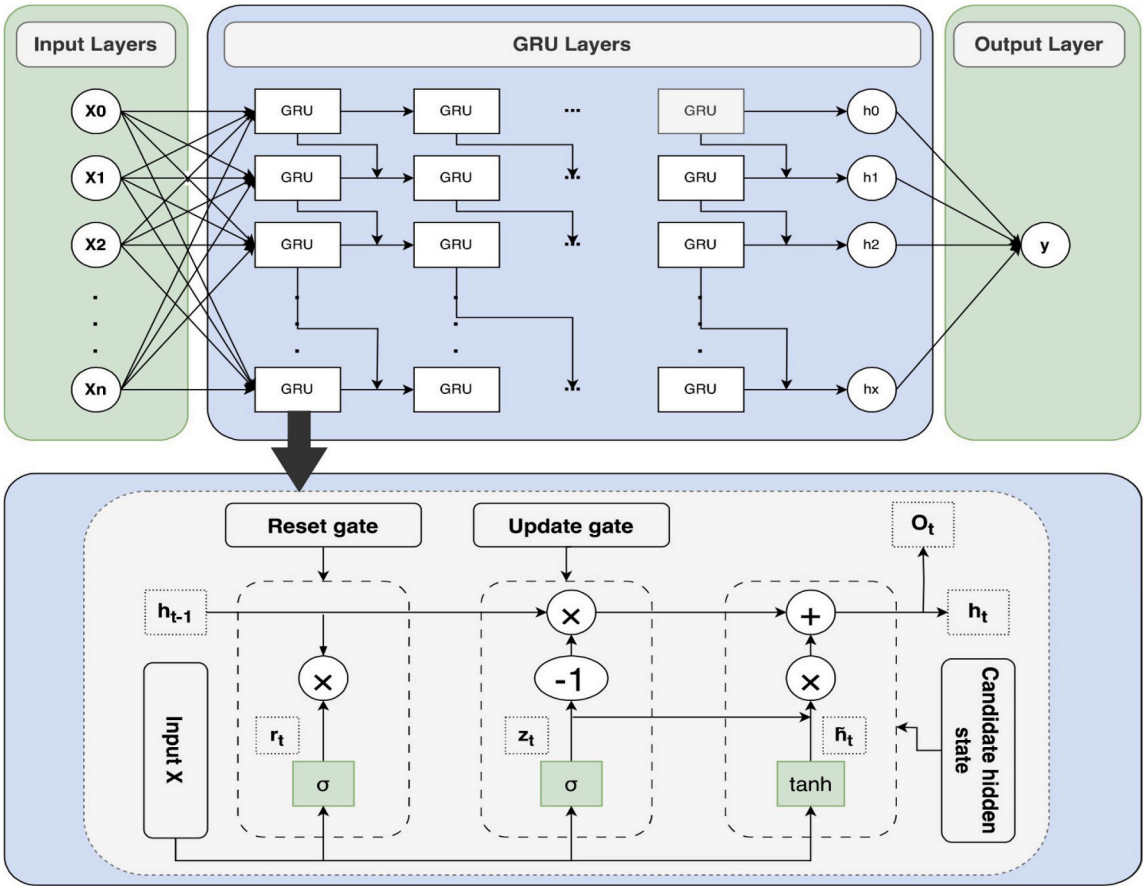


**Fig. 4.** A sample architecture of a Gated Recurrent Unit (GRU).

function is set to (tanh) for these eight layers. It is a non-linear function that maps its input to a range between −1 and 1. The formula for the (tanh) activation function is:

$$tanh(x) = \frac{e^{x} - e^{-x}}{e^{x} + e^{-x}} \tag{5}$$

### 3.6. Metrics

The effectiveness of regression models is assessed by measuring the mean difference between predicted and hypothesized values. There are various criteria for evaluating such models. We have used MSE, MAE, RMSE, and R-squared to evaluate our models. The Mean Squared Error (MSE) is a widely employed measure for assessing regression model performance. It involves determining the squared difference between predicted and actual values. The formula for calculating the MSE is as follows Eq. 6:

$$MSE = \frac{1}{n}\sum_{i=1}^{n}(y_i - \widehat{y}_i)^2 \tag{6}$$

Here, $y_i$ represents the predicted value, and $\widehat{y}_i$ is the observed value.

The Mean Absolute Error (MAE) is a common metric for evaluating how close the predicted value is to the actual absolute value. It is calculated by averaging the absolute differences between the actual and predicted values. MAE is calculated using the formula based on Eq. 7.

$$MAE = \frac{1}{n}\sum_{i=1}^{n} | y_i - \widehat{y}_i | \tag{7}$$

Root Mean Square Error (RMSE) is a metric that measures the average distance between the predicted and actual values of a regression model. It is calculated by taking the square root of the sum of the squared differences between the predicted and observed values. The formula to calculate RMSE is based on Eq. 8.

$$RMSE = \sqrt{\frac{1}{n}\sum_{i=1}^{n}(y_i - \widehat{y}_i)^2} \tag{8}$$

The R-squared metric calculates the portion of the variance in the dependent variable explained by the model. This value ranges from 0 to 1, where 1 is considered acceptable, indicating a strong relationship. However, a score of 0 indicates no relationship between the independent and dependent variables Eq. 9.

$$R^2 = 1 - \frac{\sum_{i=1}^{n}(y_i - \widehat{y}_i)^2}{\sum_{i=1}^{n}(y_i - \overline{y})^2} \tag{9}$$

## 4. Results

### 4.1. Study about European cities based on Köppen climate classification

A comparative analysis of the mean heights of buildings in various European locations, categorized according to distinct Koppen climate types, is illustrated in the box plot in Fig. 5. It is worth mentioning that the climate type Cfa, which is classified as humid subtropical, demonstrates a substantial variation in building height, with a mean of approximately 40 m and a maximum of 80 m. This observation implies a propensity for longer structures, potentially driven by the need to house denser populations or as a cultural inclination in areas characterized by temperate winters and scorching, humid summers. Csa and Csb, which correspond to Mediterranean climates characterized by warm to hot, arid summers and moderate to chilly, rainy winters, respectively, exhibit median

**Table 3**
Summary of Layers and Parameters.

| Layer (type) | Output Shape | Param # |
|---|---|---|
| gru (GRU) | (None, 1, 1024) | 3,182,592 |
| gru_1 (GRU) | (None, 1, 512) | 2,362,368 |
| gru_2 (GRU) | (None, 1, 256) | 591,360 |
| gru_3 (GRU) | (None, 1, 128) | 148,224 |
| gru_4 (GRU) | (None, 1, 64) | 37,248 |
| gru_5 (GRU) | (None, 1, 32) | 9408 |
| gru_6 (GRU) | (None, 1, 32) | 6336 |
| gru_7 (GRU) | (None, 16) | 2400 |
| dense_8 (Dense) | (None, 1) | 17 |
| **Total params:** | 6,339,953 | |
| **Trainable params:** | 6,339,953 | |
| **Non-trainable params:** | 0 | |

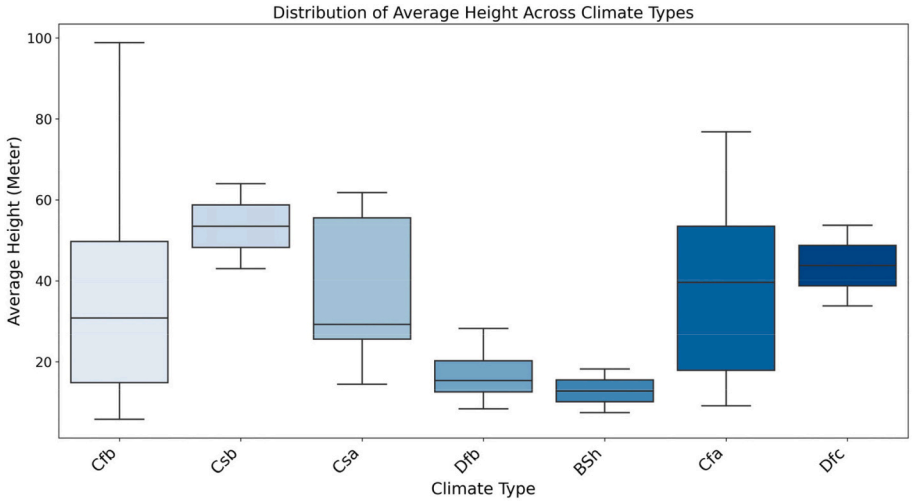


**Fig. 5.** A Box Plot for average height across countries based on Köppen climate classification.

building heights of 20 to 30 m. The median height, which is moderate in nature, is indicative of architectural styles that place an emphasis on natural ventilation and sun shading in order to mitigate the intense summer heat and accommodate the temperate winter conditions. The median height in the Dfb climate type, which is characterized by mild summers and humid continental conditions, is approximately 20 m. This climate type is expected to favor building designs that effectively retain heat and can endure the more severe seasonal fluctuations. The BSh climate type, denoting a semi-arid environment, suggests that the median building height may be as low as 20 m. This could potentially serve as a strategic maneuver to optimize thermal efficiency and water conservation in a desiccated setting. Moreover, the Dfc climate type, characterized by subarctic conditions, exhibits a comparable median height, indicating a potential inclination towards lower structures that mitigate the impact of severe winter conditions and potentially aid in heat preservation. (See Fig. 6 shows us the same trend for Avreage Volume for cities a cross climate change.)

The box plot presented in Fig. 7 provides a comprehensive illustration of the variation in green space ratios among European cities characterized by distinct Koppen climate types. The median green space ratios for the Mediterranean climate types (Csa and Csb) are approximately 5 square meters, with the Csa climate type demonstrating a marginally greater degree of variability. This may indicate the ways in which communities situated in milder climates have adapted to preserve vegetation in the face of water scarcity issues. The temperate oceanic climate (Cfb) is characterized by a potentially higher median green space ratio than 10 square meters, which suggests a more favorable setting for the preservation of such areas. Some cities in the humid continental climate (Dfb) have green space ratios approaching 20 square meters, indicating a potential for greater availability of expansive land areas designated for parks and natural spaces, as well as a diversity in urban planning strategies. Conversely, the semi-arid climate (BSh) exhibits a notably diminished median, thereby emphasizing the limitations that water resources impose on the growth of vegetation in urban areas.

The box diagram in Fig. 8 analysis illustrates the variation in building density between Koppen climate types-classified European

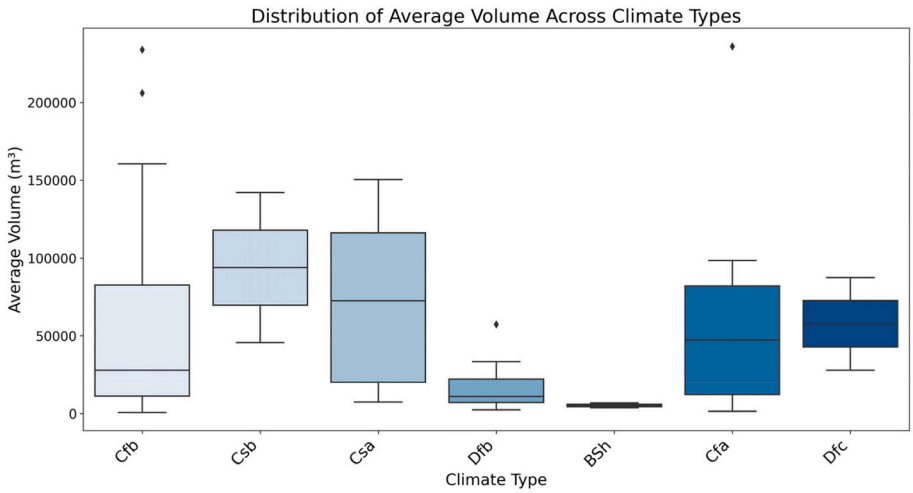


**Fig. 6.** A Box Plot for average volume countries based on Köppen climate classification.

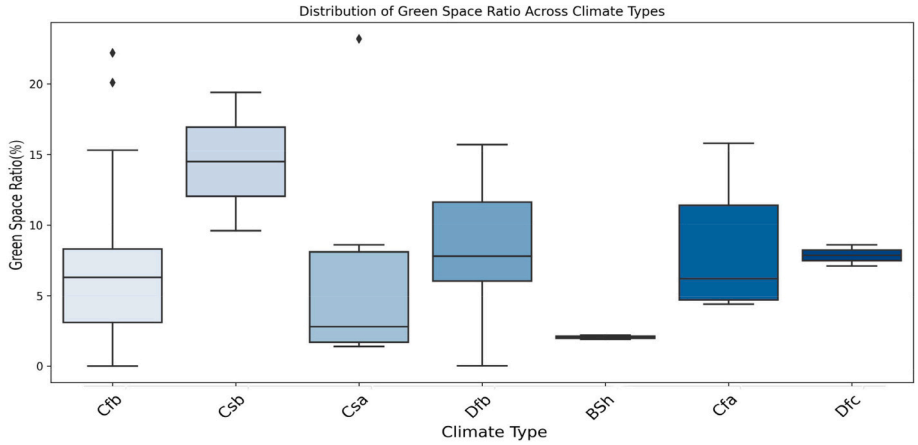


**Fig. 7.** A Box Plot for green space countries based on Köppen climate classification. (For interpretation of the references to colour in this figure legend, the reader is referred to the web version of this article.)

cities. This metric is of the utmost importance for urban sustainability, as it affects the socioeconomic structure of municipalities as well as the UHI phenomenon. The temperate oceanic climate (Cfb) is characterized by a lower median building density, probably below 40%. This may indicate a preference for urban design that strikes a balance between developed and undeveloped regions, possibly to accommodate the moderate climate devoid of an arid season. The Mediterranean climates (Csa and Csb) are characterized by median densities of at least 50%, which may indicate that urban planning in these arid summer regions prioritizes space preservation. The humid continental climate (Dfb) exhibits a diverse array of building densities, surpassing 60% in certain urban areas. This phenomenon may illustrate the wide array of urban planning strategies, which span from compact city centers to expansive suburban expansion. In distinct contrast, the median building density in the semi-arid climate (BSh) is considerably lower, suggesting that urban form may need to be modified to accommodate limited water resources and, potentially, that UHI effects could be mitigated through the development of lower-density areas.

### *4.2. Data analysis in European countries*

The study identified three independent variables of considerable importance in forecasting the intensity of UHI phenomena in urban environments: building density, green space, and average height. These morphological characteristics aid in the reduction of the UHI phenomenon. Fig. 9 illustrates the average building height by country, providing a clear comparison across a diverse set of locations. Germany tops the chart with an imposing average height of 94.27 m, indicative of its robust urban skyline. France follows, with structures averaging 57.40 m, while Italy's buildings stand at an average of 44.93 m, suggesting a preference for moderately tall buildings in these countries. Notably, buildings in Denmark and Poland share an identical average height of 38.47 m, reflecting similar urban development patterns. On the lower end of the spectrum, Cyprus exhibits the shortest buildings among the countries analyzed,

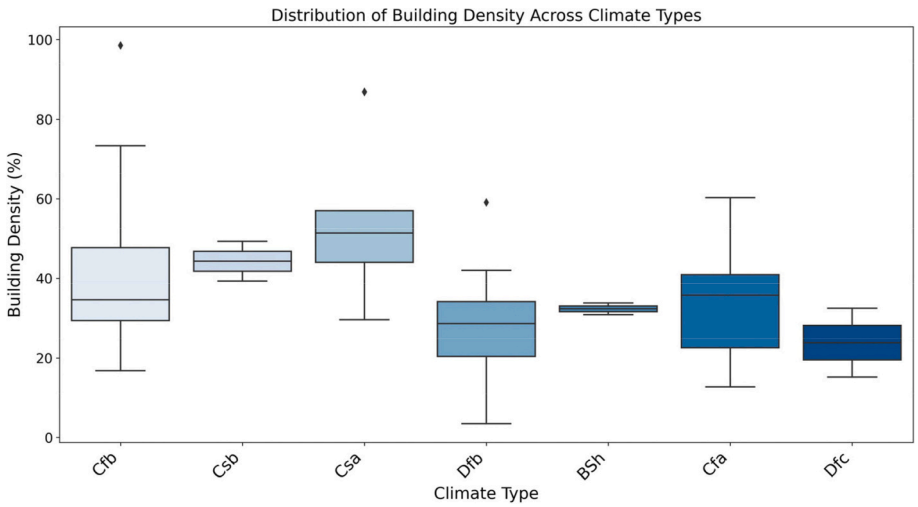


**Fig. 8.** A Box Plot for building density countries based on Köppen climate classification.

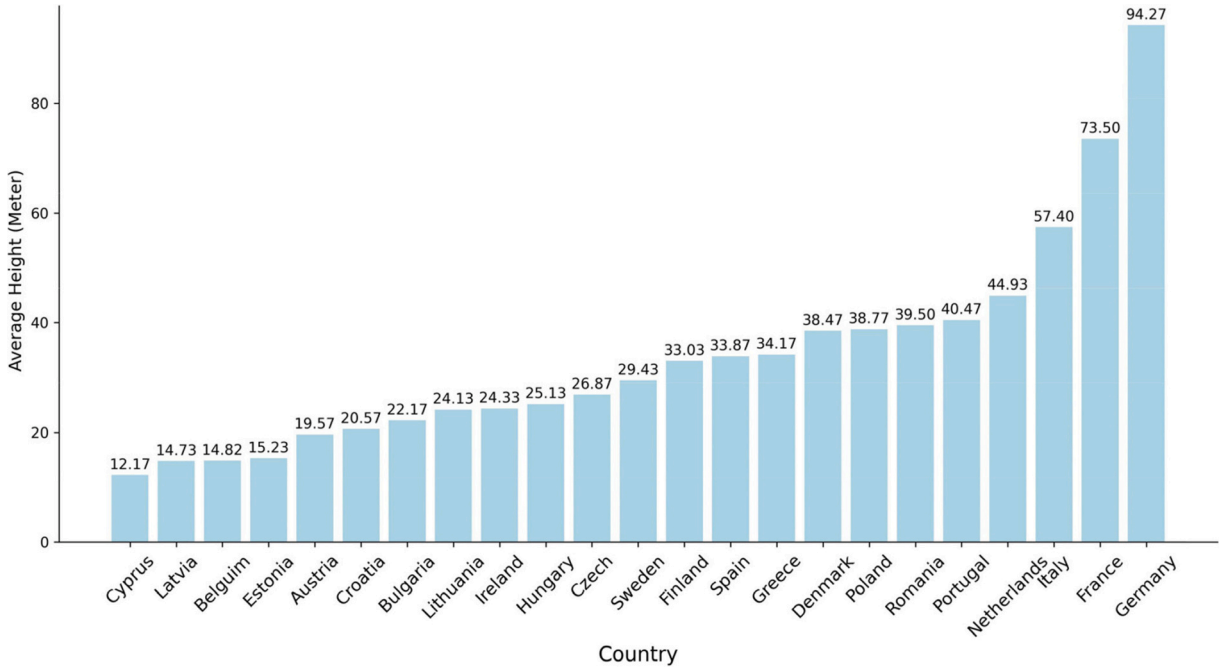


**Fig. 9.** A bar Plot for average height across countries.

with an average height of just 12.17 m, pointing to a landscape dominated by low-rise structures. The variation in building heights across countries captured in this chart not only reflects the architectural styles and urban planning strategies prevalent in each country but may also provide insights into the respective UHI effects these nations may experience.

Fig. 10 presents a comparison of average building density by country, a significant factor influencing urban spatial structure and, potentially, the UHI effect. Spain leads with the highest density, where buildings occupy 72.60% of urban space, indicative of highly compact city designs. France and Austria follow, with densities of 58.27% and 46.93%, respectively, suggesting a preference for dense

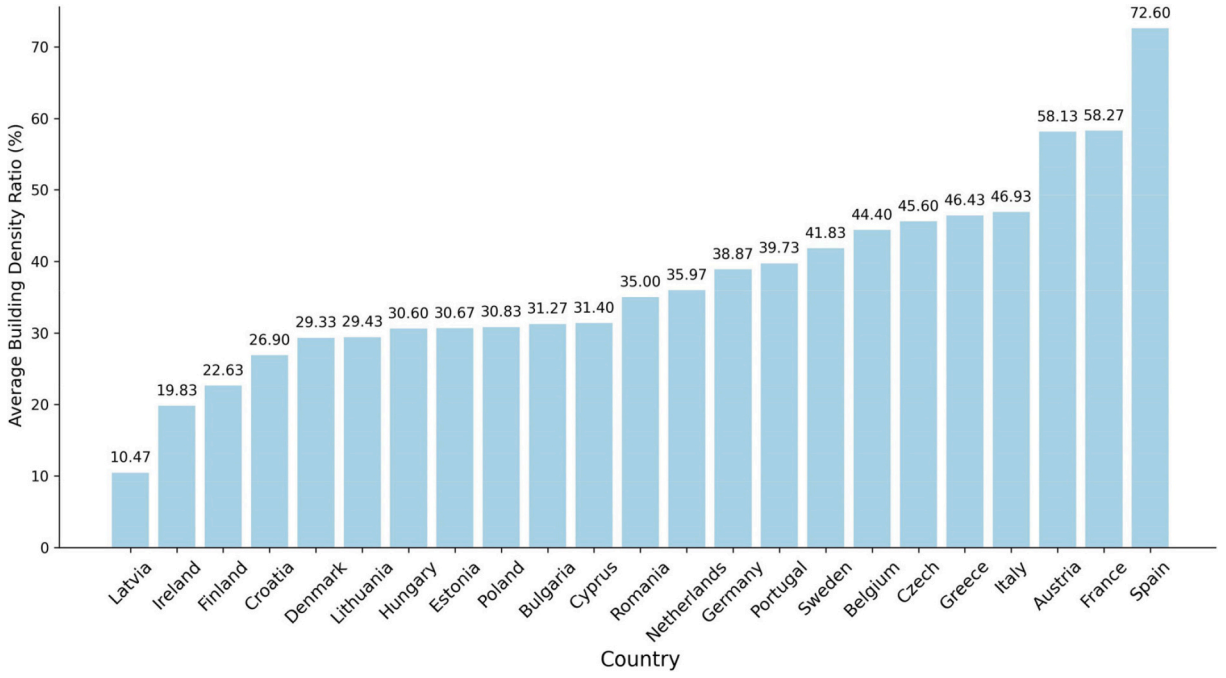


**Fig. 10.** A bar Plot for average building density across countries.

urbanization that may impact local microclimates and contribute to UHI. Meanwhile, Latvia sits at the opposite end of the spectrum with the lowest recorded building density of 10.47%, pointing to more open urban layouts that could facilitate better air circulation and potentially lessen UHI effects.

Fig. 11 provides a comparative analysis of the average green space ratio by country, which is a vital indicator of urban environmental quality and a key element in mitigating the UHI effect. The Czech Republic stands out with the highest green space ratio at 12.37%, indicating a strong emphasis on integrating natural landscapes into urban planning. This is in stark contrast to Greece, which has the lowest ratio at 1.90%, suggesting a potential area for improvement in urban green infrastructure. Countries like Spain, Estonia, and Portugal also exhibit high ratios, surpassing 10%, which could contribute positively to their urban climate regulation. Such disparities in green space allocation highlight the varying approaches to urban planning across Europe and underscore the importance of green space in enhancing urban livability and environmental sustainability.

This study considers another important independent variable such as the average volume of buildings. Within the research scope, Milan stands out with the highest recorded building volume among the examined cities, reaching an impressive 23,6024.1 cubic meters. In contrast, Dobele displays the lowest average building volume among the studied cities, with a measured quantity of 1551.5 cubic meters. In comparison to other European countries, Germany stands out due to its notably high average building volume (184,549.4 cubic meters) and building height (94.2 m). These figures may suggest that the country has undergone more substantial urbanization, leading to a potentially greater intensity of UHI effects. Cyprus and Austria, in contrast, exhibit significantly lower building volumes (4216.6 and 44,306.5 cubic meters, respectively) and heights (12.1 and 19.5 m, respectively). This indicates less densely populated urban areas, which may result in less noticeable UHI effects. The variations emphasize how the size and concentration of urban buildings may greatly impact the weather conditions in a certain area.

The Unoccupied-Area offers a compelling insight into the phenomenon of urban expansion and its impact on the UHI effect. Portugal and Italy include extensive Unoccupied-Area, measuring 1.670000e+06 and 1.857807e+06 square meters, respectively. These areas have the potential to facilitate the dissipation of heat, hence mitigating the impacts of HI. Conversely, smaller vacant spaces in nations such as Austria and Cyprus might result in more pronounced UHI effects because of the clustering of urban buildings Table 4. This component of urban design highlights the need of taking into account open and empty places in reducing the impact of the UHI phenomenon.

### 4.3. Urban Heat Island classification

The graph depicted in Fig. 12 illustrates the UHIs across various cities. To facilitate discussion and classification based on their UHI values, three distinct categories are introduced.

**High UHI Cities (Consistently above 2.0 °C):** These cities exhibit an average UHIs consistently surpassing 2.0 °C. Factors such as dense urban structures, limited greenery, and other contributors accentuate the UHI effect. Major metropolitan areas like Bucharest, Madrid, and Milan, characterized by dense populations and extensive urbanization, fall into this category. Additionally, some cities,

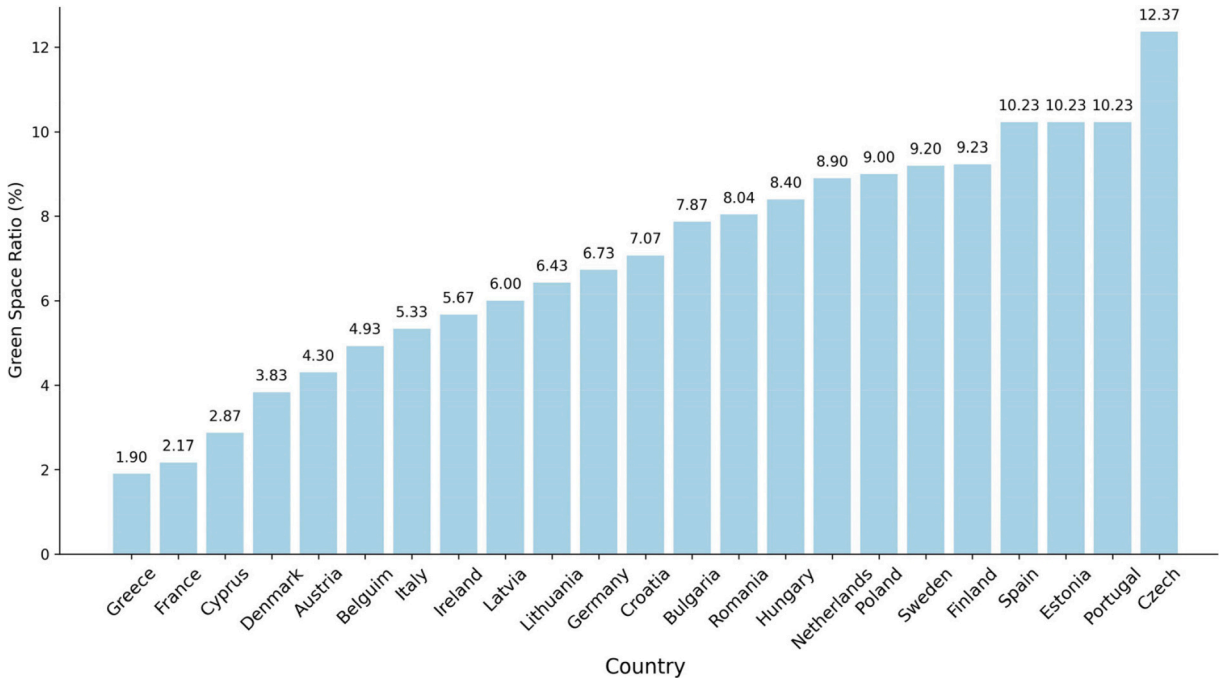


**Fig. 11.** A bar Plot for average green space ratio across countries.

**Table 4**
Descriptive table of urban texture variables for all countries.

| Country | Describe | Average-Volume ($m^3$) | Green-Space (%) | Average-Height (m) | Building-Density (%) | Unoccupied-Area ($m^2$) |
|---|---|---|---|---|---|---|
| Austria | MEAN | 44,306.5 | 4.3 | 19.5 | 58.1 | 800,277.4 |
| | STD | 34,855.9 | 0.9 | 4.51 | 28.85 | 98,717.6 |
| Sweden | MEAN | 59,259.9 | 9.2 | 29.4 | 41.4 | 621,064.5 |
| | STD | 18,262 | 1.4 | 6.7 | 12.5 | 94,586.7 |
| Germany | MEAN | 184,549.4 | 6.7 | 94.2 | 38.8 | 7.375614e+05 |
| | STD | 34,941 | 2.6 | 5.5 | 9 | 2.443510e+05 |
| Spain | MEAN | 134,425.8 | 10.2 | 33.8 | 72.6 | 1.219635e+06 |
| | STD | 21,808 | 9.3 | 7.7 | 20.2 | 3.694472e+05 |
| Greece | MEAN | 25,394.5 | 1.9 | 34.1 | 46.4 | 483,182.5 |
| | STD | 22,863 | 0.6 | 15.1 | 12 | 346,160 |
| Belgium | MEAN | 22,077.3 | 4.9 | 14.9 | 44.4 | 7.692546e+05 |
| | STD | 11,346.5 | 3.1 | 3.6 | 6.9 | 4.757637e+05 |
| Hungary | MEAN | 39,218.5 | 8.4 | 25.1 | 30.6 | 529,223.6 |
| | STD | 41,955.8 | 4.6 | 11.1 | 4.3 | 151,488 |
| Bulgaria | MEAN | 17,379.4 | 7.8 | 22.1 | 31.2 | 790,948.8 |
| | STD | 7504.8 | 3.9 | 6.5 | 13.6 | 163,258.2 |
| Ireland | MEAN | 9443.3 | 5.6 | 24.3 | 19.8 | 7.466109e+05 |
| | STD | 6209.5 | 1.8 | 13.6 | 3 | 4.643381e+05 |
| Croatia | MEAN | 12,916.8 | 7 | 20.5 | 26.9 | 522,330.7 |
| | STD | 10,100.5 | 0.4 | 10.9 | 7.4 | 212,426.6 |
| Italy | MEAN | 118,597.6 | 5.3 | 57.4 | 46.9 | 1.857807e+06 |
| | STD | 83,668.6 | 2.9 | 15.2 | 11.7 | 1.018106e+06 |
| Cyprus | MEAN | 4216.6 | 2.8 | 12.1 | 31.4 | 127,869.9 |
| | STD | 1889.4 | 1.1 | 4.4 | 1.7 | 316,161.6 |
| Latvia | MEAN | 11,867.7 | 6 | 14.7 | 10.4 | 228,132.9 |
| | STD | 13,193.2 | 1.1 | 4.7 | 4.9 | 53,272.1 |
| Czech | MEAN | 60,470.6 | 1.7 | 26.8 | 0.6 | 601,873.1 |
| | STD | 60,820.4 | 2.3 | 17.3 | 13.7 | 44,214.3 |
| Lithuania | MEAN | 22,499.7 | 6.4 | 24.1 | 29.4 | 7.363059e+05 |
| | STD | 9134.2 | 6.5 | 5.8 | 6.5 | 5.978445e+05 |
| Denmark | MEAN | 30,897.8 | 3.8 | 38.4 | 29.3 | 512,032.1 |
| | STD | 19,457.8 | 2.7 | 20.6 | 6.9 | 218,706 |
| Estonia | MEAN | 8150.9 | 10.2 | 15.2 | 30.6 | 8.789998e+05 |
| | STD | 4584.2 | 3.9 | 3.9 | 7 | 5.724105e+05 |
| Netherlands | MEAN | 50,286.1 | 8.9 | 44.9 | 35.9 | 475,009.3 |
| | STD | 53,378.7 | 9.4 | 32.8 | 9.4 | 225,697 |
| Poland | MEAN | 37,194.8 | 9 | 38.7 | 30.8 | 9.099596e+05 |
| | STD | 24,392.7 | 2.5 | 24.7 | 11.3 | 2.546469e+05 |
| Finland | MEAN | 45,199.7 | 9.2 | 33 | 22.6 | 8.165247e+05 |
| | STD | 30,080.5 | 2 | 17.1 | 7.2 | 2.176157e+05 |
| Portugal | MEAN | 69,220.1 | 12.3 | 40.4 | 39.7 | 1.670000e+06 |
| | STD | 52,532.3 | 5 | 20.3 | 7.6 | 1.589579e+05 |
| Romania | MEAN | 30,655.6 | 8 | 39.5 | 35 | 659,404.3 |
| | STD | 25,165.8 | 6.4 | 19.7 | 12.5 | 81,306.3 |
| France | MEAN | 156,314.3 | 2.1 | 73.5 | 58.2 | 478,405.6 |
| | STD | 37,364.6 | 0.3 | 9.5 | 10.6 | 252,692.5 |

situated inland without the moderating influence of large water bodies, experience a more pronounced UHI effect. For instance, Madrid, centrally located in Spain, lacks coastal temperature moderation.

**Moderate UHI Cities (1 °C to 2 °C):** Cities in this category demonstrate UHI values fluctuating between approximately 1.0 °C and 2.0 °C. Mediterranean cities like Valencia, marked by hot, dry summers, may experience an exacerbated UHI effect. However, sea breezes play a moderating role. Industrial cities like Linz, despite significant urban development, benefit from careful planning and the presence of the Danube River, which moderates temperatures. Vienna, with its urban density, is known for green spaces and parks that mitigate UHI to some extent.

**Low UHI Cities (Below 1 °C):** Cities in this group exhibit UHIs below 1.0 °C. Coastal cities such as Ostend and Faro benefit from the ocean's moderating effect, equalizing temperature differences. Cities in northern latitudes, including Stockholm, Roskilde, Tampere, Oulu, and Helsinki, have naturally cooler climates contributing to lower UHI values. The presence of ample green spaces and effective urban planning, as seen in cities like Dublin and Copenhagen, further reduces the UHI effect.

To assess potential UHI changes in the future, the study focuses on a subset of cities representing various UHI levels for 2050 and 2080 predictions. Fig. 13 compares UHI intensities across three periods: historical averages from 2007 to 2021, projections for 2050, and projections for 2080. This selection of ten cities enables a comparative examination of UHI changes over time within different UHI baselines.

A clear upward trend in UHIs is observed for every city over time. UHIs is projected to be higher in 2050 than the historical average, with further increases expected by 2080. This indicates a general intensification of the heat island effect in urban areas. While most cities will experience increased UHIs, the degree of increase varies. For example, Dublin's UHI remains consistent across the three

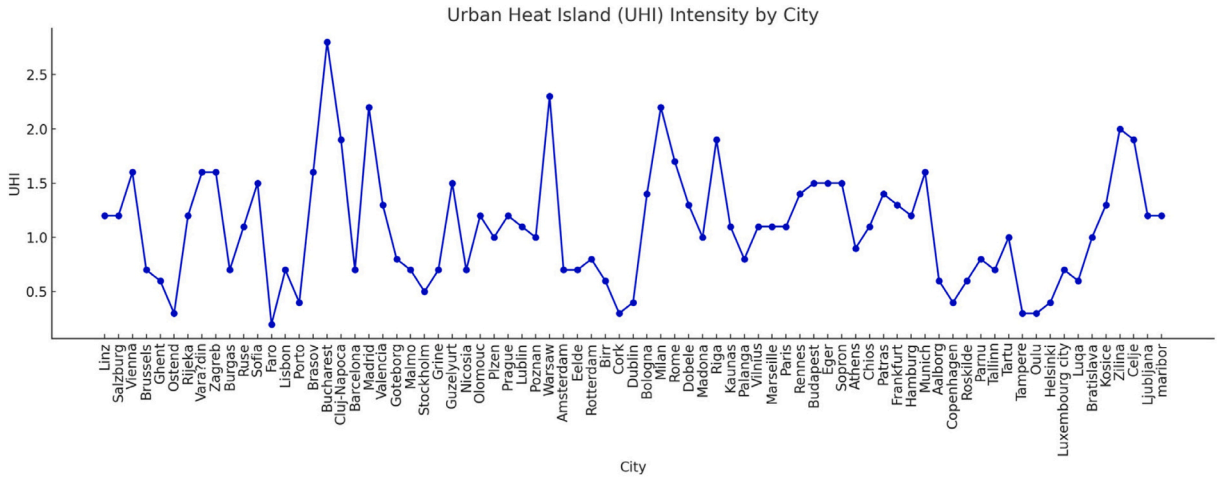


**Fig. 12.** Showing a plot of UHI intensity in various cities.

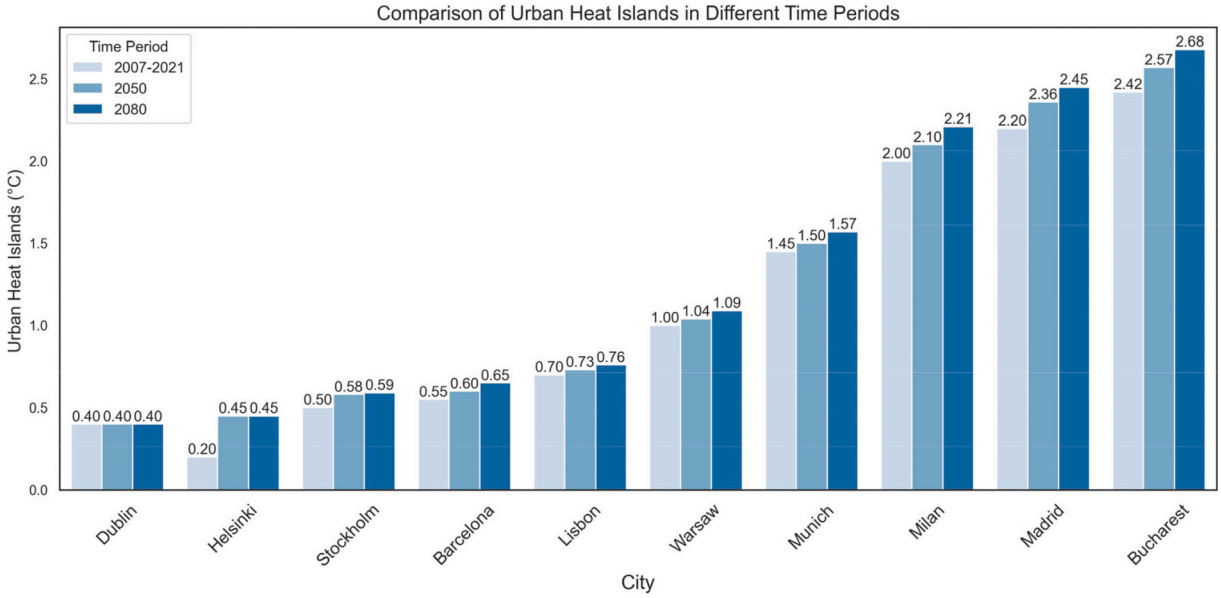


**Fig. 13.** The comparison of UHI intensity for selected cities across three different periods (Urban Weather Generator).

periods, whereas Bucharest is expected to see a notable jump from 2.42 °C to 2.68 °C by 2080. Cities like Bucharest, Milan, and Madrid, with particularly high UHIs, may face significant challenges and require substantial mitigation efforts.

### *4.4. The effect of urban heat island on CDD and HDD*

The data presented in Fig. 14 highlights a disparity between CDD values derived from the epw data and those adjusted for predicted UHI effects. As depicted in Fig. 3, all CDD values factoring in the predicted UHI consistently surpass their epw-based counterparts, indicating that the epw data tends to underestimate CDD values. This can be explained by epw (EnergyPlus Weather) data not always fully accounting for the localized warming effects of UHI. By incorporating the UHI effect, the CDD calculations appear to be more accurate and reflective of real-world conditions.

As can be seen in Fig. 14, for some of these cities (i.e., Bucharest, Milan, Madrid, Patras, Guzelyurt), the differences between CDD values from the epw data and those adjusted for UHI effects are >120. The large differences observed in these cities indicate a more pronounced UHI effect, as studied above. These cities are densely populated, industrially developed, and characterized by extensive urban development and dense infrastructure.

Similarly, the findings illustrated in Fig. 14 reveal a difference between HDD values discovered from epw data and those modified to account for anticipated UHI effects. As evident in Fig. 12, when considering the predicted UHI, the HDD values consistently fall

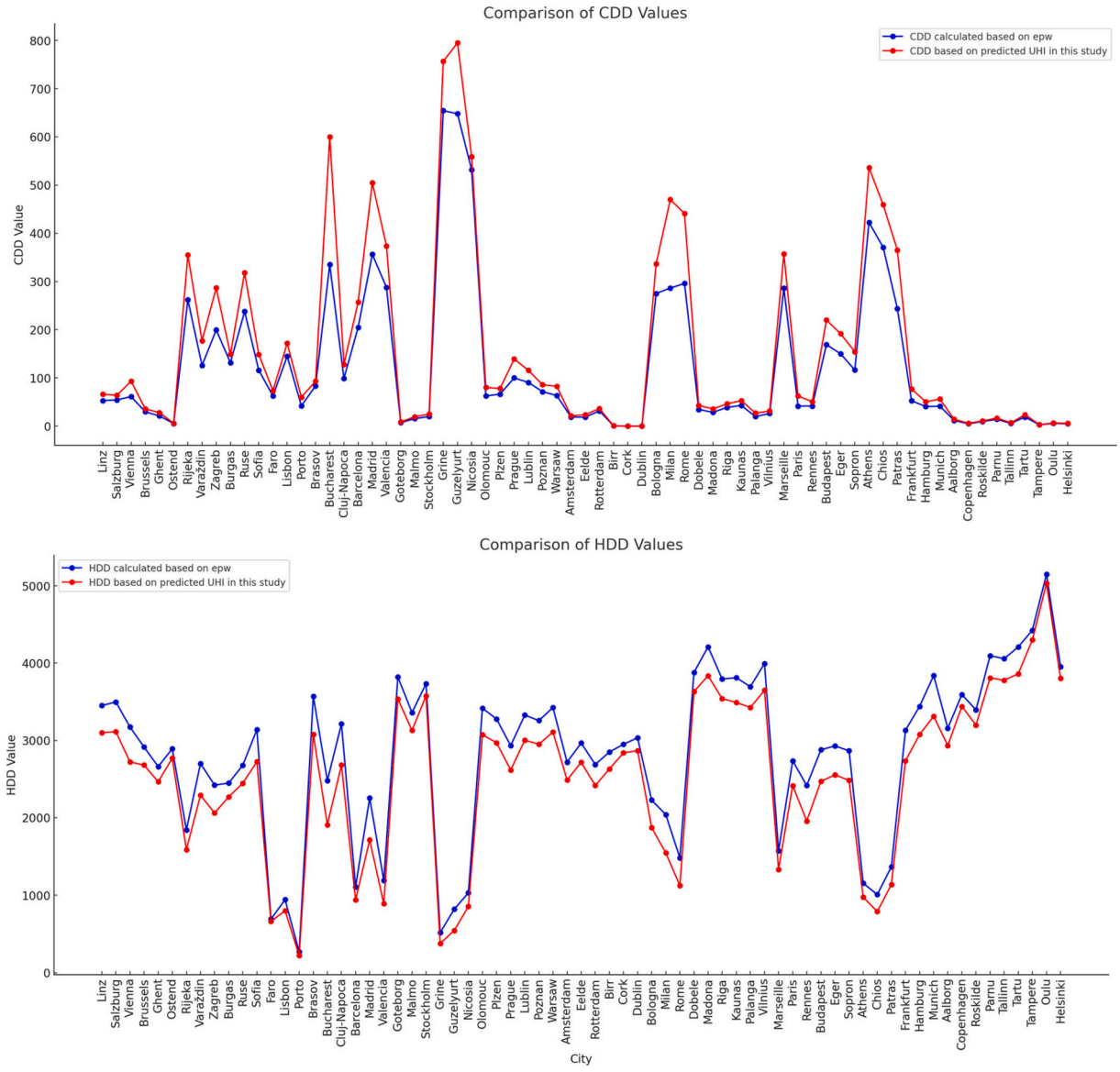


**Fig. 14.** CDD and HDD values derived from the epw data.

**Table 5**
Comparison between Urban Heat Island Simulations (UWG) and DL model(GRU) forecasts.

| City | 2007–2021 (UWG) | 2007–2021 (GRU) | 2050 (UWG) | 2050 (GRU) | 2080 (UWG) | 2080(GRU) |
|---|---|---|---|---|---|---|
| Dublin | 0.40 °C | 0.40 °C | 0.40 °C | 0.41 °C | 0.40 °C | 0.41 °C |
| Helsinki | 0.20 °C | 0.20 °C | 0.45 °C | 0.46 °C | 0.45 °C | 0.46 °C |
| Stockholm | 0.50 °C | 0.50 °C | 0.58 °C | 0.59 °C | 0.59 °C | 0.60 °C |
| Barcelona | 0.55 °C | 0.55 °C | 0.60 °C | 0.61 °C | 0.65 °C | 0.66 °C |
| Lisbon | 0.70 °C | 0.70 °C | 0.73 °C | 0.74 °C | 0.76 °C | 0.77 °C |
| Warsaw | 1.00 °C | 1.00 °C | 1.04 °C | 1.05 °C | 1.09 °C | 1.10 °C |
| Munich | 1.45 °C | 1.45 °C | 1.50 °C | 1.51 °C | 1.57 °C | 1.58 °C |
| Milan | 2.00 °C | 2.00 °C | 2.10 °C | 2.11 °C | 2.21 °C | 2.22 °C |
| Madrid | 2.20 °C | 2.20 °C | 2.36 °C | 2.37 °C | 2.45 °C | 2.46 °C |
| Bucharest | 2.42 °C | 2.42 °C | 2.57 °C | 2.58 °C | 2.68 °C | 2.69 °C |

below those derived from epw. This suggests that the epw data may be overrepresenting the heating demand. For several cities (i.e., Bucharest, Cluj-Napoca, Madrid, Milan, Brasov), this difference is >490 HDD, which can be justified by significant urbanization and dense infrastructure contributing to a stronger UHI effect, leading to warmer conditions and therefore a lower HDD when considering UHI.

Bucharest, Milan, and Madrid are noticeable for their high values, indicating that these cities may be particularly challenged by the UHI effect and may require significant mitigation efforts. The increased UHI effect observed in Bucharest, Milan, and Madrid has led to pronounced discrepancies in the values of CDD and HDD when comparing standard energy plus weather (epw) data with calculations that account for UHI variations.

Table 5 displays a comparative analysis of UHIs projections for eight European cities. However, future forecasts for 2050 and 2080 show a consistent 0.01 difference between the UWG and GRU predictions, suggesting a nuanced understanding of the DL model. The forecasts were generated using both the UWG simulations and DL model predictions using GRU. The data includes historical records from 2007 to 2021, as well as future forecasts for 2050 and 2080. Significantly, both approaches predict comparable UHI magnitudes for cities such as Dublin (0.40 to 0.41) and Helsinki (0.20 to 0.46) throughout various time periods. The future forecasts for 2050 and 2080 suggest a progressive escalation in the intensity of UHI, particularly in Milan and Bucharest, where considerable increases of up to 2.22 and 2.69 are expected, respectively. These changes reflect the expected effects of urbanization and climate change. The constant pattern seen in several locations, ranging from Dublin with little increases to Bucharest with more substantial increases, highlights the increasing difficulty posed by UHI and the promise of DL models in predicting urban climate.

### 4.5. Deep learning performance: Gated recurrent unit

The effectiveness of the proposed GRU model was assessed using four metrics. The GRU model exhibited strong accuracy in predicting UHIs within the study area, achieving a MSE of 0.003, MAE of 0.04, RMSE of 0.06, and an R-squared value of 0.92. In the initial phase of the study, a comparison among four DL models revealed that the GRU model outperformed others in prediction accuracy. The research gathered data on morphological features, topography, building height, building density, green space, building volume, occupied area, and unoccupied area. Various methods, including land use maps, digital elevation models, and OpenStreetMap, were employed to collect these data. Descriptive Table 4 outlines the mean and standard deviation values for each variable, providing an overview of the characteristics of the countries under examination.

Following the completion of the training process, four DL models undergo evaluation and analysis in three distinct modes. Initially, their status during training, as well as the values of the cost functions on the training data, are examined. Subsequently, the validation data is assessed, and the testing data is evaluated. The first model achieved the lowest error, recording 0.0122 at the end of 50 epochs. The second and third models exhibited minimum errors of 0.0085 and 0.0078, respectively. Notably, the fourth model, a GRU model, outperformed the others by achieving a minimum error of 0.0042 at the conclusion of 50 epochs Table 6. The training graph of the GRU model illustrates minimal fluctuation between the training error and the validation error. This model demonstrated superior performance, attaining an error of approximately 0.004, surpassing the outcomes of the other three models by the end of 50 epochs Fig. 15.The GRU's exceptional performance implies the potential presence of temporal or sequential patterns within the UHI data, which GRUs, as a variant of recurrent neural networks, are especially adept at capturing (Han et al., 2021).

In the second phase, we assessed the models using four metrics: MSE, MAE, RMSE, and R-squared. The results for the four models are summarized Table 7, with the GRU-based networks showing the best performance. The low loss value of 0.003 indicates minimal prediction errors and high accuracy, closely matching actual values. This is supported by the MSE of 0.003, signifying the model's ability to accurately capture data patterns. The R-squared value of 0.92 is an essential indicator, ranging from 0 to 1, where 1 is an ideal match. An R-squared of 0.92 suggests that the model's predictions explain about 92% of the variance in UHI data, demonstrating a strong correlation with actual UHIs measurements. Additionally, the RMSE and MAE are reported as 0.06 and 0.04, respectively.The Actual vs. Predicted UHI graph for the best models is shown in Fig. 16.

### 4.6. Cross validation of the models

In the third stage, we validate our trained models using data from eight additional cities (Luxembourg City, Luqa, Bratislava, Kosice, Zilina, Celje, Ljubljana, and Maribor) in our study. The validation process is of paramount importance as it allows us to assess the accuracy and applicability of our models across diverse urban environments. The comparative analysis of UHI intensities, as calculated by both the UWG and the GRU models, is summarized in Table 8 of our paper. This comparison offers valuable insights into both HDD and CDD across multiple cities. Of particular significance is the consistency observed in the UHI values derived from both the UWG and GRU models, which lends substantial support to the reliability of our modeling methodology. For instance, in Luqa, Malta,

**Table 6**
Loss value for training, validation and testing dataset.

| Model | Training Loss | Validation Loss | Testing Loss |
|---|---|---|---|
| GRU | 0.0042 | 0.0043 | 0.0039 |
| DNN | 0.0078 | 0.0078 | 0.0077 |
| Two-layer ANN | 0.0085 | 0.0085 | 0.0085 |
| One-layer ANN | 0.0122 | 0.0121 | 0.0121 |

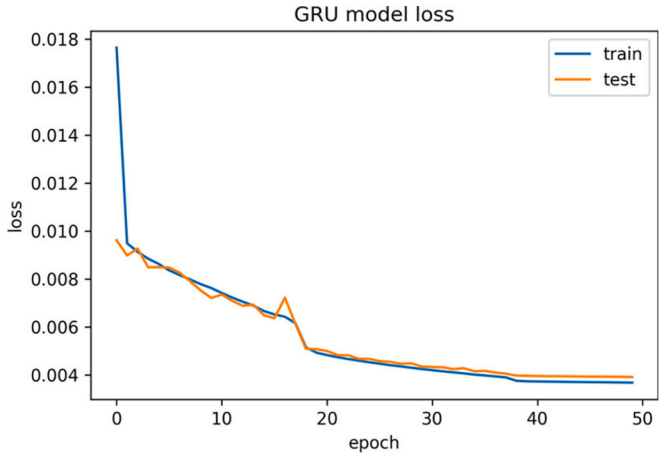


**Fig. 15.** Model Loss.

**Table 7**
Comparison between four models.

| Metrics | GRU | DNN | Two-layer ANN | One-layer ANN |
|---|---|---|---|---|
| MAE | 0.04 | 0.06 | 0.07 | 0.08 |
| MSE | 0.003 | 0.007 | 0.008 | 0.010 |
| RMSE | 0.06 | 0.08 | 0.09 | 0.10 |
| $R^2$ | 0.92 | 0.84 | 0.82 | 0.75 |

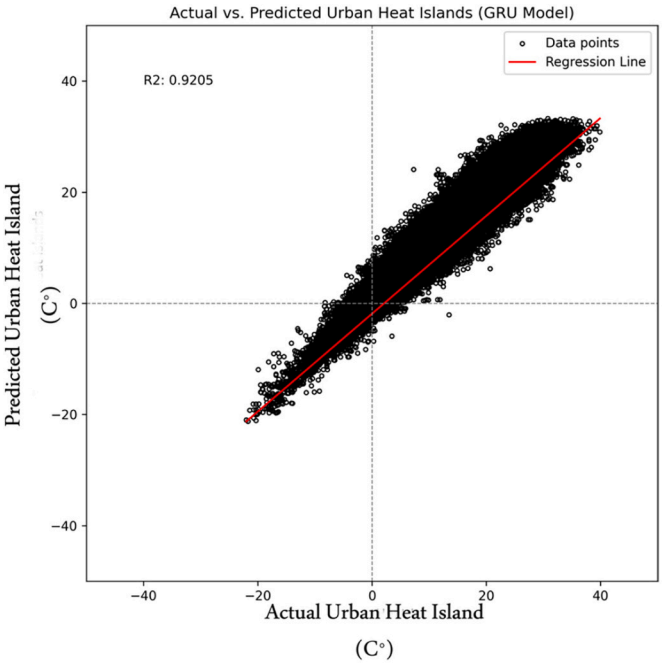


**Fig. 16.** The best model.

the UWG and GRU models yielded UHI intensities of 0.58 °C and 0.59 °C, respectively. Similarly, both models predicted UHI intensities slightly above 1 °C in Bratislava, Slovakia. This trend persisted across every city, demonstrating a close alignment between the models. For example, in Zilina, Slovakia, the GRU model predicted a UHIs just 0.01 °C greater than that of the UWG model. Consistent patterns were observed in Luxembourg City and Slovenian localities such as Celje, Ljubljana, and Maribor, with the GRU model consistently generating values within one hundredth of a degree Celsius of the UWG model's findings. The minor fluctuations observed fall within

**Table 8**
Cross-Validated UHI Intensity Comparison Across Cities.

| Country | City | CDD | HDD | UHI (UWG) | UHI (GRU) |
|---|---|---|---|---|---|
| Malta | Luqa | 496.7 | 568.8 | 0.58 °C | 0.59 °C |
| Slovakia | Bratislava | 164.2 | 2579.7 | 1.03 °C | 1.04 °C |
| Slovakia | Kosice | 121.9 | 2790.6 | 1.20 °C | 1.21 °C |
| Slovakia | Zilina | 94.9 | 2823.5 | 2.01 °C | 2.02 °C |
| Luxembourg | Luxembourg city | 36.2 | 2833.3 | 0.71 °C | 0.72 °C |
| Slovenia | Celje | 152.3 | 2470.4 | 1.95 °C | 1.96 °C |
| Slovenia | Ljubljana | 234.4 | 2271.7 | 1.80 °C | 1.81 °C |
| Slovenia | Maribor | 170.6 | 2401.2 | 1.74 °C | 1.75 °C |

the expected ranges, further affirming the reliability of both the UWG and GRU models for evaluating UHIs. These results significantly contribute to our understanding of the UHI effect, offering a validated method for its quantification across diverse urban settings.

### *4.7. SHAP sensitivity analysis*

As shown in Fig. 17, our investigation focuses on the understanding of SHAP values, which offer quantitative insights into the impact of diverse urban characteristics on the UHI effect. Every data point along the horizontal axis signifies the influence of a distinct urban feature on the output of the model. The visual representation of these impacts is provided by the distribution and density of these data points. A greater concentration of data points situated beyond the zero line signifies a more pronounced impact on the predictions generated by the model. By designating red points to indicate high feature values and blue points to represent low feature values, it becomes possible to evaluate the impact of feature value magnitudes on the UHI effect.

Specific characteristics exhibit discernible patterns in relation to their SHAP values. One example of this is the clear adverse effect that green space has on UHI intensity in urban environments, as evidenced by the high concentration of SHAP values in the negative range. This indicates that expanding green space is a viable strategy for reducing the intensity of UHI. On the other hand, the SHAP values for average volume and building density are overwhelmingly positive, suggesting that the UHI effect is typically exacerbated by greater building densities and larger building volumes. The occupied area is an additional characteristic that exhibits this pattern, in which an elevated proportion of the urban landscape that is enclosed by structures correlates with a heightened intensity of UHI.

Conversely, certain characteristics show a more intricate correlation with the UHI effect. An illustration of this can be seen in the nearly equal distribution of positive and negative SHAP values for the azimuth angle of buildings. This suggests that the orientation of the buildings influences UHIs in a variable manner, potentially as a result of interactions with other elements or particular regional circumstances. In a similar vein, the average height demonstrates both positive and negative SHAP values; however, the greater magnitude of the positive values indicates that elevated structures might be a contributing factor to increased UHIs. The predominantly negative impact of characteristics such as facade-to-site ratio suggests that a greater facade area in relation to the site could potentially aid in diminishing UHIs. The lack of a discernible trend in the X and Y point coordinates suggests that the spatial position within the urban grid might not exert a consistent or substantial influence on the intensity of UHI throughout the output of the model. Insofar as climate mitigation is concerned, these insights underline the significance of an integrated approach to urban planning and design by emphasizing the multifaceted character of urban features that influence UHI.

Expanding upon the in-depth examination of SHAP values that was previously deliberated, the chart presented in Fig. 17 provides a concise overview of the mean influence of every urban feature on the model's output, thereby presenting a concise synopsis of their

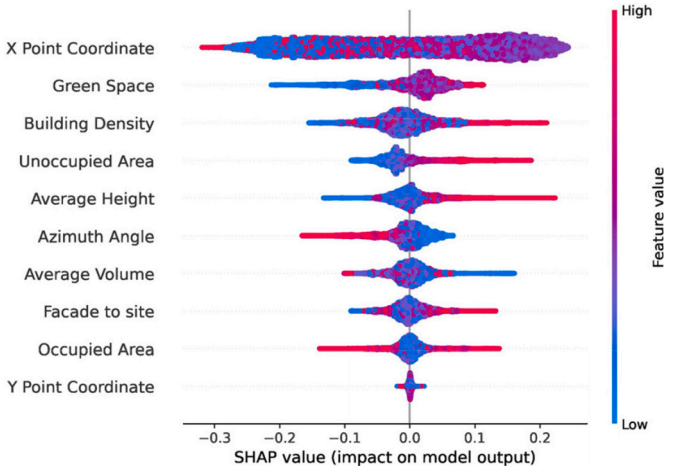


**Fig. 17.** SHAP Value Analysis of Urban Features Affecting HUI intensity.

respective significance. The visual depiction validates that the 'X Point Coordinate' exerts the most significant average influence on predictions of the UHI effect, despite the fact that its precise impact continues to be intricate. The terms 'Green Space' and'Unoccupied Area' demonstrate a significantly adverse average impact, thereby emphasizing their functions in alleviating the UHI effect. On the other hand, the mean impacts of'Building Density,' 'Average Height,' 'Average Volume,' and'Occupied Area' are all positive, which is consistent with the earlier assertion that urban structures that are denser and taller have the potential to increase UHIs. The variables 'Azimuth Angle' and'Facade to Site' exhibit a moderate and diverse influence on the UHI phenomenon, whereas the'Y Point Coordinate' demonstrates the least average impact, implying that its impact is negligible or inconsistent. The comprehensive perspective presented here highlights the intricate interplay between urban design elements and the microclimatic fluctuations they generate.

## 5. Discussion

### 5.1. Urban morphology affects urban heat island

Examining UHIs in urban areas provides valuable insights for developing strategies to mitigate and counteract the UHI phenomenon. This issue holds significant importance in the field of urban planning and design, enabling the creation of effective approaches to address the adverse impacts of rising temperatures in urban environments. Moreover, in Europe, the weather in cities is influenced by large-scale atmospheric circulation systems, such as sea breezes (Xoplaki et al., 2012; Grundstrom et al., 2015). This interaction exhibits variations on a daily, monthly, and annual basis, dependent on prevailing synoptic conditions. To investigate and accurately predict such a complex interplay, a fundamental question to address is: which parameters should be considered? A multitude of variables, including city coordinates (Soltanifard and Aliabadi, 2019), proximity to the ocean (Yun et al., 2020; Santamouris et al., 2017), vegetation (Susca et al., 2011), wind direction (Sen and Roesler, 2020), building density (Li et al., 2020), and layout (Yang et al., 2010), among others, emerge as potential factors. DL algorithms could assist in weighting their impact. To contextualize our findings within a broader analysis of UHIs, it is essential to review and incorporate relevant studies conducted by other researchers. For example, Han et al. created an approach utilizing RNN to generate precise weather forecasts using readily accessible, generic files (Han et al., 2021). Similarly, (Tariku and Gharib Mombeni, 2023) Tariku et al. developed application of an ANN-based method for generating hourly urban canopy temperature and local wind speed for energy simulation based on urban morphology and characteristics. In another study, Otaghsara et al. focused on modeling the Surface Urban Heat Island (SUHI) in Santa Rosa, California, USA, utilizing remote sensing data, urban morphology parameters, and partial least squares (PLS) regression (Taheri Otaghsara and Arefi, 2019). In contrast, our research predominantly relies on urban morphological features to predict UHIs. Notably, many prior studies in this field are regionally confined, often concentrating on specific areas or countries. In contrast, our study encompasses multiple cities in the European region, providing a more comprehensive understanding of the relationship between urban morphological features and UHIs.

Yun et al. employed weather data obtained from a Sydney, Australia weather station covering the period from 1999 to 2017 (Yun et al., 2020). In contrast, our study relies on simulated data gathered from various locations across Europe spanning the years 2007 to 2021. By underscoring this distinction in both data sources and duration, we make a valuable contribution to the current body of knowledge in the analysis of UHIs. This also underscores the distinctiveness of our methodology. Incorporating citations and references from these relevant studies underscores the significance and innovation of our research within the wider academic dialogue on predicting UHIs during the initial phases of city design. This contributes valuable insights to urban planning and design considerations. The study highlights the potential efficacy of a GRU model in predicting UHIs. Throughout the training and testing phases, the model demonstrated commendable generalization, signifying its ability to effectively address the over-fitting challenges commonly encountered in time series models like LSTM and RNN.

### 5.2. The innovation of research

Previous research focused on Forecasting UHIs values for specific locations in individual countries, such as the United States, Iran, Australia, and Canada (Taheri Otaghsara and Arefi, 2019; Debbage and Shepherd, 2015; Yun et al., 2020; Tariku and Gharib Mombeni, 2023; Faraji et al., 2022). On the other hand, the present study takes a broader approach by examining the UHI in 69 separate places in the European continent in the time frames (2007–2021) and predicting the UHI phenomenon for 2050 and 2080 by the Climate Change World Weather Generator tool (CCWorldWeatherGen) (Jentsch et al., 2013). In addition, This study has investigated the HDD and the CDD during the occurrence of the UHI phenomenon, which directly impacts the energy consumption of the building. These extensive analyses provide a deeper understanding of the relationship between the UHI phenomenon and urban morphology, which significantly contributes to the development and promotion of urban planning in the early stages of city design to control this phenomenon and global warming. This research emphasizes the importance of considering variables such as green space and building density when estimating the intensity of UHI in the initial stages of design in urban contexts Fig. 17, that one of the ways to reduce UHIs is to increase green space and reduce building density in urban areas. Green space, such as trees, vegetation, and green roofs, can provide cooling effects by shading heat-absorbing surfaces, deflecting solar radiation, and releasing moisture into the atmosphere. On the other hand, building density can affect airflow and ventilation in urban areas, which leads to the reduction of air pollution in cities. By predicting the intensity of the UHI and optimizing the balance between green space, building density, and other morphological features studied in this research, urban planners can design more sustainable and livable cities that reduce these negative effects. The approach of this research increases our understanding of the determining factors of the UHIs in urban texture, which is very important in controlling climate change, improving human health, and reducing air pollution.

### 5.3. Main findings

The assessment and prediction of UHIs using the UWG tools and the GRU model have yielded valuable insights into the correlation between UHIs and various urban design features across different cities. This research primarily concentrated on the timeframe spanning from 2007 to 2021, during which the GRU model demonstrated superior accuracy in predicting UHIs compared to three other DL models. Despite the focus on this period, UHI data were collected for the years 2050 to 2080, offering a more extensive perspective on UHI trends. Urban areas, shaped by human activities and infrastructure, tend to exhibit higher temperatures compared to their rural counterparts (Marando et al., 2022). The consequences of these temperature changes vary based on a city's geographic location and climate. Notably, cities in the Warm-Summer Humid Continental (Dfb) climate, such as Helsinki and Stockholm, did not witness an increase in UHI intensity from 1960 to 2021. In contrast, the analysis reveals that regions with a Humid Subtropical climate (Cfa), Warm Mediterranean Summer climate (Csa), and Temperate Oceanic climate (Cfb) made significant contributions, with factors like green space, building density, and average height playing pivotal roles. Fig. 13 illustrates that cities such as Madrid, Bucharest, Milan, and Munich, situated in these climates, experience higher UHIs compared to other climate zones. Projections for the years 2050 and 2080 indicate a substantial increase in UHIs in these cities, leading to elevated Cooling Degree Days Fig. 14. This phenomenon is expected to augment the energy consumption of buildings, subsequently increasing electricity costs. Yan Liul's research (Liu et al., 2020) highlights that reducing building density has a more pronounced impact on alleviating the UHI effect compared to decreasing building height. Specifically, diminishing building density results in approximately 20% and 30% reductions in High-intensity Development heat (HIdh). Another study by Fitsum Tariku (Tariku and Gharib Mombeni, 2023) discovered that the UHI effect contributes to a 23% increase in cooling energy demand and a 29% decrease in heating energy consumption. This leads to an overall 18% rise in the total energy demand for buildings in metropolitan areas. Additionally, the UHI effect leads to indoor temperatures exceeding the cooling set point by 7.6%. In summary, these findings underscore the significance of incorporating UHI considerations into urban planning and design. They also provide insight into the potential impacts of climate change and temperature increases at the metropolitan level. Such insights can serve as a foundation for promoting effective and sustainable urban development.

### 5.4. Limitations of the study

The computational resources employed in this study followed specific hardware specifications. The processor, an Intel(R) Core(TM) i5-9400F CPU with a base clock speed of 2.90 GHz, played a crucial role in data processing. The study operated with a 16.0 GB RAM capacity, and a NVIDIA GEFORCE GTX 1050 TI GPU was employed for computational tasks related to the research. These well-defined hardware specifications significantly contributed to data processing, training four different models, and conducting analyses, particularly those linked to the GRU model in this study. The effective collaboration between the CPU, GPU, and sufficient RAM ensured swift model execution, allowing for the exploration of intricate relationships between urban morphologies and UHIs. It's important to underscore that the specific hardware configuration mentioned may impact the processing speed and overall performance of the four models, especially the GRU model. The choice of computing resources for this research was based on the model's requirements and the available resources during the study. Offering detailed information about the hardware configurations aims to provide a comprehensive understanding of the computational environment in which the GRU model was developed and tested. One constraint encountered during the study was the absence of suitable EPW (EnergyPlus Weather) data for the cities in the focus, namely Luxembourg and Malta. Given the limitations of our current dataset, the unavailability of EPW files restricted our capacity to broaden the scope to include these cities. To address this limitation, collaboration with meteorological organizations and weather forecasters is essential to gather or generate suitable EPW data for comprehensive coverage of cities and countries.

## 6. Conclusion

As UHIs continue to threaten urban health, energy use, comfort, and general well-being, the need for effective tools to analyze and predict UHI behavior in European cities is becoming more critical. We demonstrate the effectiveness of deep learning techniques in meeting this need, providing a strong foundation for policymakers to develop specific mitigation plans. Moreover, pinpointing the elements of urban texture associated with UHI offers essential insights for urban planning strategies to mitigate UHI impacts. Additionally, we also show the vital importance of prioritizing green infrastructure in urban planning efforts, enabling data-driven decisions and promoting cross-sectoral cooperation to create more resilient, and sustainable cities. The study's results provide actionable insights and evidence-based recommendations for policymakers, urban planners, and other stakeholders to tackle the challenges presented by UHIs and support sustainable urban development. By using such information in urban planning and policy strategies, cities can more effectively address the challenges of UHI and climate change. Our approach enhances the development of more sustainable and resilient urban environments for future generations in European cities.

## CRediT authorship contribution statement

**Alireza Attarhay Tehrani:** Software, Resources, Project administration, Methodology, Investigation, Formal analysis, Data curation, Conceptualization. **Omid Veisi:** Writing – review & editing, Writing – original draft, Visualization, Validation, Supervision, Resources, Project administration, Methodology, Formal analysis, Conceptualization. **Kambiz kia:** Writing – review & editing, Writing – original draft, Conceptualization. **Yasin Delavar:** Writing – review & editing, Writing – original draft. **Sasan Bahrami:** Writing – review & editing, Writing – original draft. **Saeideh Sobhaninia:** Writing – review & editing, Supervision. **Asma Mehan:** Writing –

review & editing, Supervision.

## Declaration of competing interest

The authors declare that they have no known competing financial interests or personal relationships that could have influenced the work reported in this paper.

## Data availability

Data will be made available on request.

## Appendix A. Supplementary data

Supplementary data to this article can be found online at https://doi.org/10.1016/j.uclim.2024.102061.

## References


Addas, A., 2023. Machine learning techniques to map the impact of urban heat island: investigating the city of Jeddah. Land 12, 1159.

Ahmed, Z., Zafar, M.W., Ali, S., et al., 2020. Linking urbanization, human capital, and the ecological footprint in g7 countries: an empirical analysis. Sustain. Cities Soc. 55, 102064.

Allam, Z., Dhunny, Z.A., 2019. On big data, artificial intelligence and smart cities. Cities 89, 80–91.

Alonso, L., Renard, F., 2020. A new approach for understanding urban microclimate by integrating complementary predictors at different scales in regression and machine learning models. Remote Sens. 12, 2434.

Arnfield, A.J., 2003. Two decades of urban climate research: a review of turbulence, exchanges of energy and water, and the urban heat island. Int. J. Climatol. 23, 1–26.

Assaf, G., Hu, X., Assaad, R.H., 2023. Predicting urban heat island severity on the census-tract level using bayesian networks. Sustain. Cities Soc. 97, 104756.

Boned Fustel, P., Cuesta Peredo, C., Boned-Ombuena, A., Carreiro, G., Fustel Rodríguez, M., 2021. Climate change and the city: analysis of the urban heat island effect on mortality in valencia, Spain. Eur. J. Pub. Health 31 ckab164–633.

Boukhabla, M., Alkama, D., Bouchair, A., 2013. The effect of urban morphology on urban heat island in the city of Biskra in Algeria. International Journal of Ambient Energy 34, 100–110.

Burry, M., Kolarevic, B., 2003. Between intuition and process: parametric design and rapid prototyping. Architecture in the Digital Age: Design and Manufacturing 148–162.

Cao, X., Onishi, A., Chen, J., Imura, H., 2010. Quantifying the cool island intensity of urban parks using aster and ikonos data. Landsc. Urban Plan. 96, 224–231.

Chang, C.-R., Li, M.-H., Chang, S.-D., 2007. A preliminary study on the local cool-island intensity of Taipei City parks. Landsc. Urban Plan. 80, 386–395.

Cho, K., Van Merriënboer, B., Gulcehre, C., Bahdanau, D., Bougares, F., Schwenk, H., Bengio, Y., 2014. Learning phrase representations using rnn encoder-decoder for statistical machine translation, arXiv preprint arXiv:1406.1078.

Debbage, N., Shepherd, J.M., 2015. The urban heat island effect and city contiguity. Comput. Environ. Urban. Syst. 54, 181–194.

Dugord, P.-A., Lauf, S., Schuster, C., Kleinschmit, B., 2014. Land use patterns, temperature distribution, and potential heat stress risk–the case study berlin, Germany. Comput. Environ. Urban. Syst. 48, 86–98.

Faisal, A.F., Rahman, A., Habib, M.T.M., Siddique, A.H., Hasan, M., Khan, M.M., 2022. Neural networks based multivariate time series forecasting of solar radiation using meteorological data of different cities of Bangladesh. Results in Engineering 13, 100365.

Fallah Madvari, R., 2022. Artificial intelligence (ai), machine learning (ml) and deep learning (dl) on health, safety and environment (hse), archives of. Occup. Health 6, 1321–1322.

Faraji, M., Nadi, S., Ghaffarpasand, O., Homayoni, S., Downey, K., 2022. An integrated 3d cnn-gru deep learning method for short-term prediction of pm2. 5 concentration in urban environment. Sci. Total Environ. 834, 155324.

Fitria, R., Kim, D., Baik, J., Choi, M., 2019. Impact of biophysical mechanisms on urban heat island associated with climate variation and urban morphology. Sci. Rep. 9, 19503.

Fleischmann, M., 2019. Momepy: urban morphology measuring toolkit. Journal of Open Source Software 4, 1807.

Giridharan, R., Ganesan, S., Lau, S., 2004. Daytime urban heat island effect in high-rise and high-density residential developments in Hong Kong. Energ. Buildings 36, 525–534.

Goodfellow, I., Bengio, Y., Courville, A., 2016. Deep Learning. MIT Press. http://www.deeplearningbook.org.

Grêt-Regamey, A., Switalski, M., Fagerholm, N., Korpilo, S., Juhola, S., Kyttä, M., Käyhkö, N., McPhearson, T., Nollert, M., Rinne, T., et al., 2021. Harnessing sensing systems towards urban sustainability transformation. npj Urban Sustainability 1, 40.

Grundstrom, M., Tang, L., Hallquist, M., Nguyen, H., Chen, D., Pleijel, H., 2015. Influence of atmospheric circulation patterns on urban air quality during the winter, atmospheric. Pollut. Res. 6, 278–285.

Guerreiro, S.B., Dawson, R.J., Kilsby, C., Lewis, E., Ford, A., 2018. Future heat-waves, droughts and floods in 571 european cities. Environ. Res. Lett. 13, 034009.

Haas, T., Olsson, K., 2014. Transmutation and reinvention of public spaces through ideals of urban planning and design. Space Cult. 17, 59–68.

Hamada, S., Ohta, T., 2010. Seasonal variations in the cooling effect of urban green areas on surrounding urban areas. Urban For. Urban Green. 9, 15–24.

Han, J.M., Ang, Y.Q., Malkawi, A., Samuelson, H.W., 2021. Using recurrent neural networks for localized weather prediction with combined use of public airport data and on-site measurements. Build. Environ. 192, 107601.

Han, Y., Zhang, K., Xu, Y., Wang, H., Chai, T., 2023. Application of parametric design in the optimization of traditional landscape architecture. Processes 11, 638.

Heaviside, C., Macintyre, H., Vardoulakis, S., 2017. The urban heat island: implications for health in a changing environment. Current Environmental Health Reports 4, 296–305.

Huang, X., Wang, Y., 2019. Investigating the effects of 3d urban morphology on the surface urban heat island effect in urban functional zones by using high-resolution remote sensing data: a case study of Wuhan, Central China. ISPRS J. Photogramm. Remote Sens. 152, 119–131.

Huang, H., Deng, X., Yang, H., Li, S., et al., 2020. Spatial evolution of the effects of urban heat island on residents' health. Tehnički vjesnik 27, 1427–1435.

Jentsch, M.F., James, P.A., Bourikas, L., Bahaj, A.S., 2013. Transforming existing weather data for worldwide locations to enable energy and building performance simulation under future climates. Renew. Energy 55, 514–524.

Kleerekoper, L., Van Esch, M., Salcedo, T.B., 2012. How to make a city climate-proof, addressing the urban heat island effect. Resour. Conserv. Recycl. 64, 30–38.

Klemm, W., Heusinkveld, B.G., Lenzholzer, S., Jacobs, M.H., Van Hove, B., 2015. Psychological and physical impact of urban green spaces on outdoor thermal comfort during summertime in the Netherlands. Build. Environ. 83, 120–128.

Lafortezza, R., Carrus, G., Sanesi, G., Davies, C., 2009. Benefits and well-being perceived by people visiting green spaces in periods of heat stress. Urban For. Urban Green. 8, 97–108.
Li, X., Zhou, Y., Yu, S., Jia, G., Li, H., Li, W., 2019. Urban heat island impacts on building energy consumption: a review of approaches and findings. Energy 174, 407–419.
Li, Y., Schubert, S., Kropp, J.P., Rybski, D., 2020. On the influence of density and morphology on the urban heat island intensity. Nat. Commun. 11, 2647.
Liao, W., Hong, T., Heo, Y., 2021. The effect of spatial heterogeneity in urban morphology on surface urban heat islands. Energ. Buildings 244, 111027.
Liu, Y., Li, Q., Yang, L., Mu, K., Zhang, M., Liu, J., 2020. Urban heat island effects of various urban morphologies under regional climate conditions. Sci. Total Environ. 743, 140589.
Liu, S., Zhang, J., Li, J., Li, Y., Zhang, J., Wu, X., 2021. Simulating and mitigating extreme urban heat island effects in a factory area based on machine learning. Build. Environ. 202, 108051.
Liu, B., Guo, X., Jiang, J., 2023. How urban morphology relates to the urban heat island effect: a multi-indicator study. Sustainability 15, 10787.
Lyu, F., Wang, S., Han, S.Y., Catlett, C., Wang, S., 2022. An integrated cybergis and machine learning framework for fine-scale prediction of urban heat island using satellite remote sensing and urban sensor network data. Urban Informatics 1, 6.
Ma, B., Zhou, T., Lei, S., Wen, Y., Htun, T.T., 2019. Effects of urban green spaces on residents' well-being. Environ. Dev. Sustain. 21, 2793–2809.
Maimaitiyiming, M., Ghulam, A., Tiyip, T., Pla, F., Latorre-Carmona, P., Halik, Ü., Sawut, M., Caetano, M., 2014. Effects of green space spatial pattern on land surface temperature: implications for sustainable urban planning and climate change adaptation. ISPRS J. Photogramm. Remote Sens. 89, 59–66.
Marando, F., Heris, M.P., Zulian, G., Udías, A., Mentaschi, L., Chrysoulakis, N., Parastatidis, D., Maes, J., 2022. Urban heat island mitigation by green infrastructure in european functional urban areas. Sustain. Cities Soc. 77, 103564.
Martin, P., Baudouin, Y., Gachon, P., 2015. An alternative method to characterize the surface urban heat island. Int. J. Biometeorol. 59, 849–861.
McCarty, D., Lee, J., Kim, H.W., 2021. Machine learning simulation of land cover impact on surface urban heat island surrounding park areas. Sustainability 13, 12678.
Mehan, A., 2023. Re-theorizing the collective action to address the climate change challenges: towards resilient and inclusive agenda. Can. J. Reg. Sci. 46, 8–15.
Mehan, A., Tafrata, B., 2023. Embedding justice in resilient climate change action. In: The Palgrave Encyclopedia of Urban and Regional Futures. Springer, pp. 484–486.
Mirzaei, P.A., 2015. Recent challenges in modeling of urban heat island. Sustain. Cities Soc. 19, 200–206.
Montávez, J.P., Rodríguez, A., Jiménez, J.I., 2000. A study of the urban heat island of Granada. Int. J. Climatol. 20, 899–911.
Monteiro, M.V., Doick, K.J., Handley, P., Peace, A., 2016. The impact of greenspace size on the extent of local nocturnal air temperature cooling in London. Urban For. Urban Green. 16, 160–169.
Mortaheb, R., Jankowski, P., 2023. Smart city re-imagined: City planning and geoai in the age of big data. Journal of Urban Management 12, 4–15.
Nastran, M., Kobal, M., Eler, K., 2019. Urban heat islands in relation to green land use in european cities. Urban For. Urban Green. 37, 33–41.
K. S. Ochoa, T. Comes, A machine learning approach for rapid disaster response based on multi-modal data, The case of housing & shelter needs (2021).
Piracha, A., Chaudhary, M.T., 2022. Urban air pollution, urban heat island and human health: a review of the literature. Sustainability 14, 9234.
Qezelbash-Chamak, J., Badamchizadeh, S., Eshghi, K., Asadi, Y., 2022. A survey of machine learning in kidney disease diagnosis. Machine Learning with Applications 10, 100418.
Rao, P., Tassinari, P., Torreggiani, D., 2023. Exploring the land-use urban heat island nexus under climate change conditions using machine learning approach: a spatio-temporal analysis of remotely sensed data. Heliyon 9.
Rizwan, A.M., Dennis, L.Y., Chunho, L., 2008. A review on the generation, determination and mitigation of urban heat island. J. Environ. Sci. 20, 120–128.
Saldana Ochoa, K., Ohlbrock, P.O., D'Acunto, P., Moosavi, V., 2021. Beyond typologies, beyond optimization: exploring novel structural forms at the interface of human and machine intelligence. Int. J. Archit. Comput. 19, 466–490.
Santamouris, M., Haddad, S., Fiorito, F., Osmond, P., Ding, L., Prasad, D., Zhai, X., Wang, R., 2017. Urban heat island and overheating characteristics in Sydney, Australia. An analysis of multiyear measurements. Sustainability 9, 712.
Schwarz, N., Lautenbach, S., Seppelt, R., 2011. Exploring indicators for quantifying surface urban heat islands of european cities with modis land surface temperatures. Remote Sens. Environ. 115, 3175–3186.
Schwarz, N., Schlink, U., Franck, U., Großmann, K., 2012. Relationship of land surface and air temperatures and its implications for quantifying urban heat island indicators–an application for the city of Leipzig (Germany). Ecol. Indic. 18, 693–704.
Sen, S., Roesler, J., 2020. Wind direction and cool surface strategies on microscale urban heat island. Urban Clim. 31, 100548.
Shahmohamadi, P., Che-Ani, A., Etessam, I., Maulud, K., Tawil, N., 2011. Healthy environment: the need to mitigate urban heat island effects on human health. Procedia Engineering 20, 61–70.
Shi, H., Xian, G., Auch, R., Gallo, K., Zhou, Q., 2021. Urban heat island and its regional impacts using remotely sensed thermal data–a review of recent developments and methodology. Land 10, 867.
Singh, N., Singh, S., Mall, R., 2020. Urban Ecology and Human Health: Implications of Urban Heat Island, Air Pollution and Climate Change nexus. In: Urban Ecology. Elsevier, pp. 317–334.
Soltanifard, H., Aliabadi, K., 2019. Impact of urban spatial configuration on land surface temperature and urban heat islands: a case study of Mashhad, Iran. Theor. Appl. Climatol. 137, 2889–2903.
Steeneveld, G.-J., Koopmans, S., Heusinkveld, B., Van Hove, L., Holtslag, A., 2011. Quantifying urban heat island effects and human comfort for cities of variable size and urban morphology in the Netherlands. J. Geophys. Res. Atmos. 116.
Stewart, I.D., 2011. A systematic review and scientific critique of methodology in modern urban heat island literature. Int. J. Climatol. 31, 200–217.
Sun, Y., Haghighat, F., Fung, B.C., 2020. A review of the-state-of-the-art in data-driven approaches for building energy prediction. Energ. Buildings 221, 110022.
Susca, T., Gaffin, S.R., Dell'Osso, G., 2011. Positive effects of vegetation: urban heat island and green roofs. Environ. Pollut. 159, 2119–2126.
Suthar, G., Kaul, N., Khandelwal, S., Singh, S., 2024. Predicting land surface temperature and examining its relationship with air pollution and urban parameters in bengaluru: a machine learning approach. Urban Clim. 53, 101830.
Taheri Otaghsara, M., Arefi, H., 2019. Modelling urban heat island using remote sensing and city morphological parameters. Int. Arch. Photogramm. Remote. Sens. Spat. Inf. Sci. 42, 1035–1040.
Tan, J., Zheng, Y., Tang, X., Guo, C., Li, L., Song, G., Zhen, X., Yuan, D., Kalkstein, A.J., Li, F., et al., 2010. The urban heat island and its impact on heat waves and human health in shanghai. Int. J. Biometeorol. 54, 75–84.
Tariku, F., Gharib Mombeni, A., 2023. Ann-based method for urban canopy temperature prediction and building energy simulation with urban heat island effect in consideration. Energies 16, 5335.
Tavares, I., Manfredini, R., Almeida, J., Soares, J., Ramos, S., Foroozandeh, Z., Vale, Z., 2022. Comparison of pv power generation forecasting in a residential building using ann and dnn. IFAC-PapersOnLine 55, 291–296.
Tehrani, A.A., Veisi, O., Fakhr, B.V., Du, D., 2024. Predicting solar radiation in the urban area: a data-driven analysis for sustainable city planning using artificial neural networking. Sustain. Cities Soc. 100, 105042.
Touchaei, A., Wang, Y., 2015. Characterizing urban heat island in Montreal (Canada)–effect of urban morphology. Sustain. Cities Soc. 19, 395–402.
Tyrväinen, L., Pauleit, S., Seeland, K., De Vries, S., 2005. Benefits and Uses of Urban Forests and Trees, Urban forests and trees: A reference book, pp. 81–114.
U. Nations, 2014. World urbanization prospects: the 2014 revision, highlights. Department of economic and social affairs. Population Division, United Nations 32.
Varentsov, M., Krinitskiy, M., Stepanenko, V., 2023. Machine learning for simulation of urban heat island dynamics based on large-scale meteorological conditions. Climate 11, 200.
Varış Husar, S.C., Mehan, A., Erkan, R., Gall, T., Allkja, L., Husar, M., Hendawy, M., 2023. What's next? Some priorities for young planning scholars to tackle tomorrow's complex challenges. Eur. Plan. Stud. 31, 2368–2384.

Veisi, O., Shakibamanesh, A., Rahbar, M., 2022. Using intelligent multi-objective optimization and artificial neural networking to achieve maximum solar radiation with minimum volume in the archetype urban block. Sustain. Cities Soc. 86, 104101.
Vergara, D., Blanco, A., Marciano Jr., J., Meneses III, S., Borlongan, N., Sabuito, A., 2023. Assessing and modelling urban heat island in Baguio city using landsat imagery and machine learning. Int. Arch. Photogramm. Remote. Sens. Spat. Inf. Sci. 48, 457–464.
Wang, S.-Y., Ou, H.-Y., Chen, P.-C., Lin, T.-P., 2024. Implementing policies to mitigate urban heat islands: analyzing urban development factors with an innovative machine learning approach. Urban Clim. 55, 101868.
Weiss, G., Goldberg, Y., Yahav, E., 2018. On the practical computational power of finite precision rnns for language recognition, arXiv preprint arXiv:1805.04908.
Wong, L.P., Alias, H., Aghamohammadi, N., Aghazadeh, S., Sulaiman, N.M.N., 2017. Urban heat island experience, control measures and health impact: a survey among working community in the city of Kuala Lumpur. Sustain. Cities Soc. 35, 660–668.
Xoplaki, E., Trigo, R.M., García-Herrera, R., Barriopedro, D., D'andrea, F., Fischer, E.M., Gimeno, L., Gouveia, C., Hernández, E., Kuglitsch, F.G., et al., 2012. Large-Scale Atmospheric Circulation Driving Extreme Climate Events in the Mediterranean and Related Impacts (Chapitre 6).
Yang, F., Lau, S.S., Qian, F., 2010. Summertime heat island intensities in three high-rise housing quarters in inner-city shanghai China: building layout, density and greenery. Build. Environ. 45, 115–134.
Yang, J., Wang, Y., Xiu, C., Xiao, X., Xia, J., Jin, C., 2020. Optimizing local climate zones to mitigate urban heat island effect in human settlements. J. Clean. Prod. 275, 123767.
Yao, Y., Chang, C., Ndayisaba, F., Wang, S., 2020. A new approach for surface urban heat island monitoring based on machine learning algorithm and spatiotemporal fusion model. IEEE Access 8, 164268–164281.
Yin, C., Yuan, M., Lu, Y., Huang, Y., Liu, Y., 2018. Effects of urban form on the urban heat island effect based on spatial regression model. Sci. Total Environ. 634, 696–704.
Yuan, C., Adelia, A.S., Mei, S., He, W., Li, X.-X., Norford, L., 2020. Mitigating intensity of urban heat island by better understanding on urban morphology and anthropogenic heat dispersion. Build. Environ. 176, 106876.
Yun, G.Y., Ngarambe, J., Duhirwe, P.N., Ulpiani, G., Paolini, R., Haddad, S., Vasilakopoulou, K., Santamouris, M., 2020. Predicting the magnitude and the characteristics of the urban heat island in coastal cities in the proximity of desert landforms. The case of Sydney. Sci. Total Environ. 709, 136068.
Zargar, S.H., Brown, N.C., 2020. Deep learning in early-stage structural performance prediction: Assessing morphological parameters for buildings. In: Proceedings of IASS Annual Symposia, volume 2020. International Association for Shell and Spatial Structures (IASS), pp. 1–13.
Zhou, X., Chen, H., 2018. Impact of urbanization-related land use land cover changes and urban morphology changes on the urban heat island phenomenon. Sci. Total Environ. 635, 1467–1476.